HHS Public Access

Author manuscript

Neuron. Author manuscript; available in PMC 2019 August 22.

Published in final edited form as:

Neuron. 2018 August 22; 99(4): 829–841.e6. doi:10.1016/j.neuron.2018.07.022.

Striatal Microstimulation Induces Persistent and Repetitive Negative Decision-Making Predicted by Striatal Beta-Band Oscillation

Ken-ichi Amemori[#1,2], **Satoko Amemori**[#1], **Daniel J. Gibson**[1], and **Ann M. Graybiel**[1,3,*]

[1]McGovern Institute for Brain Research and Department of Brain and Cognitive Sciences, Massachusetts Institute of Technology, 43 Vassar Street, Cambridge, MA 02139, USA.

[2]The Hakubi Center for Advanced Research and Primate Research Institute, Kyoto University, 41-2 Kanrin, Inuyama, Aichi 484-8506, Japan.

[3]Lead Contact

[#] These authors contributed equally to this work.

SUMMARY

Persistent thoughts inducing irrationally pessimistic and repetitive decisions are often symptoms of mood and anxiety disorders. Regional neural hyperactivities have been associated with these disorders, but it remains unclear whether there is a specific brain region causally involved in these persistent valuations. Here, we identified potential sources of such persistent states by microstimulating the striatum of macaques performing a task by which we could quantitatively estimate their subjective pessimistic states using their choices to accept or reject conflicting offers. We found that this microstimulation induced irrationally repetitive choices with negative evaluations. Local field potentials recorded in the same microstimulation sessions exhibited modulations of beta-band oscillatory activity that paralleled the persistent negative states influencing repetitive decisions. These findings demonstrate that local striatal zones can causally affect subjective states influencing persistent negative valuation, and that abnormal beta-band oscillations can be associated with persistency in valuation accompanied by an anxiety-like state.

eTOC Blurb

Amemori et al. identified candidate subcortical loci potentially related to persistency of anxiety-like states and inflexibility in OCD. The authors' work in non-human primates shows that striatal

[*]Correspondence to: Ann M. Graybiel (graybiel@mit.edu).

AUTHOR CONTRIBUTIONS

K.A., S.A. and A.M.G. designed the experiments and performed the surgeries. K.A. and S.A. collected the recording and stimulation data. K.A. and D.J.G analyzed the electrorheological data, with S.A. and A.M.G. providing critical detailed feedback. S.A. and A.M.G analyzed the anatomical data. K.A and A.M.G. wrote the manuscript; all authors edited the manuscript.

DECLARATION OF INTERESTS

The authors declare no competing interests.

stimulation induces repetitive negative choice pattern, accompanied by modulation of striatal beta oscillation.

Keywords

Primate; caudate nucleus; cost-benefit decisions; beta oscillation; emotion; motivation; macaque; basal ganglia; value judgment; approach-avoidance conflict

INTRODUCTION

Mood disorders are a major health problem worldwide, with lifetime prevalence estimates of ~20%, accounting for ~30% of the global non-fatal disease burden (Steel et al., 2014). Long-lasting mood changes are cardinal features of these disorders and are particularly resistant to conventional therapeutic approaches (Pizzagalli, 2011). Similarly, irrationally persistent thoughts inducing repetitive and pessimistic valuation are often signs and symptoms of disorders such as obsessive compulsive disorder (OCD) and OC-spectrum disorders (Boileau, 2011) with lifetime prevalence of ~3% (Ruscio et al., 2010). These irrationally persistent and anxiety-like states are an important feature of these disorders, often resistant to treatment. The underlying neuronal mechanisms inducing such persistent negative states influencing repetitive decision-making are not well understood, impeding advances in therapy.

A correlation between persistent negative states and abnormal neural activity in the human brain is documented (Pizzagalli, 2011). In the limbic circuit of patients with mood disorders, a correlation of cerebral blood flow with the symptoms has been reported (Chen et al., 2007). In computational modeling studies (Bakic et al., 2014; Eldar et al., 2016), efforts have been made to define quantitatively subjective mood-like states persistently influencing value-based decision-making (Eldar and Niv, 2015). Such a state-like process could play a crucial role in regulating flexibility and fixity in behavior (Amemori et al., 2011), and the dysfunction of the process could produce stereotyped or OCD-like symptoms (Burguiere et al., 2013). These studies raise the possibility that there could be specific neuronal features representing the mood-like state that persistently affects negative decision-making. However, the causal sources of the persistent negative valuation, and the neural signaling correlates underlying the induced persistent negative states, have remained elusive.

The caudate nucleus (CN) is one of the regions known to be involved in mood and anxiety disorders (Aupperle et al., 2011; Price and Drevets, 2012) in humans. In searching for the causal role of the CN, the primate CN has been implicated in associative learning (Williams and Eskandar, 2006) and behavioral flexibility (Graybiel, 2008; Kim and Hikosaka, 2013; Nakamura and Hikosaka, 2006; Saka et al., 2004), which require long-lasting changes in value evaluation and behavioral facilitation. However, the specific neural activity that might underlie these functions is not known. One neural activity pattern that could be associated with an anxiety-like state is beta oscillatory activity (Lipsman et al., 2014; Merkl et al., 2015), which has been suggested to maintain the current state or status quo (Engel and Fries, 2010).

We here hypothesize that the primate CN could be causally involved in the generation of persistent and repetitive negative states, and that neural activity in the CN could exhibit specific features correlated with these states. To examine these possibilities, we combined multi-site recording and microstimulation experiments in macaques performing an approach-avoidance (Ap-Av) conflict paradigm that has been used to test anxiety-like behavior in humans (Aupperle et al., 2015; Korn et al., 2017). The Ap-Av task has also been extensively used to characterize the effect of anxiolytic agents in rodents (Millan, 2003), and previously we used this task to characterize quantitatively the anxiety-like state that could influence the subjective valuation process (Amemori and Graybiel, 2012). We report that microstimulation applied to the CN of the monkeys is capable of inducing a sharp and prolonged state or states influencing pessimistic valuation, as assessed quantitatively by econometrics modeling (Train, 2003). Critically, we recorded local field potential (LFP) oscillatory activity in the CN while we manipulated the behavior of the animals to test whether modulation of CN neural activity was associated with the causal induction of persistent pessimistic states and inflexible choice patterns. Our findings suggest that local striatal circuits could be causal sources in producing persistent pessimistic states, and that striatal beta oscillation could be a neural correlate of the persistent states.

RESULTS

Behaviors in the Ap-Av Task

Two monkeys performed the Ap-Av decision-making task (STAR Methods) (Figure 1A). In the task, a compound visual cue made up of apposed red and yellow horizontal bars appeared after a 2-s precue period. The lengths of the bars varied independently over ~100 steps. The length of the red bar signaled the offered amount of liquefied food. The length of the yellow bar signaled the offered pressure of an airpuff directed at the monkey's face. After a 1.5-s cue period, two targets appeared above and below the compound cue. The monkey was required to report its decision by using a joystick within a 3-s response period to move a cursor to one or the other target. If the monkey chose the cross target (approach Ap choice), an airpuff with pressure as indicated by the yellow bar was delivered, followed by the liquefied food in an amount signaled by the red bar. When the monkey chose the square target (avoidant Av choice), no airpuff was given, but a minimal and constant amount of reward was delivered to ensure that the monkeys would perform the task. The locations of the targets were alternated randomly. The monkeys systematically varied their decisions to accept or to reject the offers, depending on the relative amounts of food and airpuff indicated by the cues (Figure 1B). The reaction times (RTs) were longer for Av choices than for Ap choices and were specifically lengthened around the decision boundary (Figure 1C).

CN Microstimulation Induced Acute Changes in Ap-Av Decisions

To perform microstimulation simultaneously with LFP recordings, we chronically implanted multiple independently movable electrodes targeting the CN (Feingold et al., 2012). During daily sessions, we selected one of 15–18 electrodes located at distributed CN sites for microstimulation (200-μs pulses delivered at 200 Hz, 70–100 μA), and the others were used for simultaneous electrophysiological recording (STAR Methods) (Figure S1A). The stimulation train was applied for 1 s at cue onset (Figure 1A). Stimulation sessions were

divided into successive blocks: *Stim-off* (trials before microstimulation), *Stim-on* (trials with microstimulation), and *Follow-up* (trials after microstimulation) blocks, each of which consisted of 150–250 trials. We performed 112 stimulation experiments (52 in monkey S and 60 in monkey P) and additionally performed 74 recording-only experiments (38 in monkey S and 36 in monkey P) to record task-related LFP signals without stimulation artifacts. In the recording-only experiments, two blocks of the Ap-Av task were separated by a block of a control approach-approach (Ap-Ap) task, in which the subjects determined their choices based on two offered reward sizes (Figure S1B). In the stimulation experiments, we calculated the difference between decision matrices for the *Stim-off* block and the other designated blocks, and measured the total change in decision frequencies as the sum of increase in Ap and that in Av (i.e., %ΔAp + %ΔAv). We set a change of 5% as the threshold to discriminate effective and non-effective sessions (STAR Methods). For the 74 recording-only sessions, the false positive rate to misclassify non-effective as effective by this criterion was less than 5% (Figures S1B–S1E). We thus defined the stimulation-induced change to be significant if the change exceeded the discrimination threshold. After we defined its significance level, we used the difference in positive and negative effects (i.e., %ΔAv − %ΔAp) to clarify the size and direction of each effect. Microstimulation at the majority of sites (74 sites, 66%) did not induce significant changes in decision during the *Stim-on* trials, whereas stimulation at nearly a quarter of the sites (25, 22%) induced an increase in Av choice (negative effect) (Figure 1D) and stimulation at 13 sites induced an increase in Ap choice (positive effect) (Figure 1E). Effective sites were widely distributed (Figure 1F). These results indicate that distributed sites in the CN are causally involved in modulating affective judgments, and can do so acutely. We designated each local site that is involved in the generation of acute negative decisions as part of a generative circuit.

To examine neuronal activity around these generative circuit sites, we recorded spike activity from the electrodes implanted around the negative effective sites during the recording-only sessions (STAR Methods) (Figures S1F–S1H). We found a spatial correlation between the negative stimulation effects and features of unit activity (Figure 1G). The proportion of units encoding upcoming Av choices (labeled N units) was significantly larger in the 1-mm bins around the negative effective sites than in other bins ($p < 0.05$, Fisher's exact test) (Figure 1G), suggesting that N units could be a part of the generative circuit. These spatial correlations are important, as they suggest a close relationship between cellular responses and the generation of acute negative effects. By contrast, the distribution of units encoding upcoming Ap choices (labeled P units) did not exhibit such a spatial correspondence with the negative effective sites (Figure 1G).

CN Microstimulation Induced Persistent Pessimistic State

We next asked whether these effects of microstimulation could be persistent. We defined 41 sessions as significantly effective by the 5% threshold. We then asked whether the effects of the CN microstimulation persisted after we stopped the microstimulation (Figure 2A). To exclude fully any remaining influence of preceding stimulation effects, we focused on 33 sites at which the CN microstimulation induced a significant change in choice behavior in the current session without having had any detectable effect in the previous session. Among these 33 experiments, we observed negative effects, defined as an increase in Av choices, in

the *Stim-on* blocks of 23 sites (70%). Positive effects, defined as increases in Ap choices, were observed at 10 sites (30%). The negative effects were sustained in the *Follow-up* blocks for over three-quarters of the negative sites (18/23, 78%). By contrast, positive effects were maintained in the *Follow-up* blocks for only one site (1/10, 10%). Thus, unlike nearly all of the positive effects, the negative effects induced by the CN microstimulation tended to exhibit a persistent character, suggesting a potential role of these CN sites in the induction of persistent states of pessimistic mood.

In one positive and 18 negative sessions, the choice pattern did not recover in the *Follow-up* block. After these sessions, to characterize the extent of this remaining influence, we continued to perform a no-stimulation experiment (*Extended session*) until the choice pattern returned to baseline. Each of the *Extended sessions* was separated into three 200-trial blocks, and the changes from the *Stim-off* block were calculated for these blocks. We designated the first block in the *Extended session* in which the effect size fell below the 5% discrimination threshold as the *Recovery* block (Figure 2A). The effect disappeared during the first *Extended session* in 16 experiments, but in three experiments, second *Extended sessions* were needed before the effects fully disappeared (Figure 2B). Thus, microstimulation at some CN sites can have effects lingering beyond the stimulation block of 200–250 trials and even into at least the following day.

CN Microstimulation Influenced Cost-Benefit Integration

To quantify the state that appeared to influence the value evaluation of the monkeys (Eldar et al., 2016), we needed a computational model that characterizes quantitatively the monkeys' subjective valuation process. To accomplish this, we introduced econometrics modeling (Train, 2003). For the choice behaviors in each block, we performed logistic regression to produce the model, which derived the approximate boundary between Ap and Av choices (i.e., the decision boundary) (Figure 2C). To compare the stimulation effects on different choice patterns, we performed a normalization procedure to align data on a standard decision boundary (Figure S2A). We then searched for major features of the positive and negative effects, focusing on how they affected the pattern of decision-making. We examined the stimulation-induced changes in x-intercept and the intersection between the decision boundary with $y = 100$, where y indicates the offered airpuff (i.e., intersection with $y = 100$) (Figure 2D). We found no significant changes in the x-intercepts ($p > 0.05$, t-test) for either effective or non-effective sessions, but the intersections with $y = 100$ decreased in positive sessions and increased in negative sessions with significance values of $p < 0.001$ (t-test). Specific changes in the intersection with $y = 100$ indicate that the effective stimulation consistently changed the slope without any parallel shift of the decision boundary. We then examined the time course of the effects by separating the *Stim-on* block into 4 temporal periods and deriving the decision boundary for each period. The slope did not change in non-effective sessions, but the slopes in the positive and negative sessions respectively increased and decreased gradually over the course of the *Stim-on* block (Figure 2D). These results suggest that both positive and negative stimulations accumulated their effects and specifically affected the slope of the decision boundaries.

Importantly, as the reciprocal of the slope corresponds to the cost-benefit ratio (i.e., the ratio of the sensitivities to reward and airpuff, CBR) in the econometrics modeling (STAR Methods), the negative stimulation could specifically increase the monkey's subjective CBR. We therefore examined how the CBR changed across the 23 negative effective sessions from the *Stim-on* to *Recovery* blocks. We found a tight correlation ($r = 0.57$, $p < 0.001$, Pearson's correlation coefficients) between increased Av choices and the size of change in the CBR (Figure 2E), suggesting that the monkeys emphasized the negative value of the airpuff over the positive value of the food reward during the decision periods of the *Stim-on* and *Follow-up* blocks.

To test whether anxiolytic treatment could block the negative effects (STAR Methods), we performed additional microstimulation experiments (Figures 2F and S2B). After the first 200-trial block without stimulation (*Stim-off*), we applied microstimulation (150 μA) in the second (*Stim-on*) and third (*Stim-on* + *diazepam*) blocks. Between the second and third blocks, we administered diazepam (0.25 mg/kg, IM). Diazepam significantly suppressed all negative effects ($p < 0.05$, t-test), suggesting a possible relationship of the negative effect to a potential anxiety-like state. We also performed another set of control experiments to confirm that the microstimulation did not induce eye movements (STAR Methods), excluding a potential influence of detectable stimulation-induced movement (Figure S2C). Nor did we observe any other stimulation-related movements (Figures S3A–S3G). In summary, the negative effect of CN microstimulation at the effective sites influenced the CBR, changing the monkeys' valuation to emphasize punishment over reward, and anxiolytic treatment blocked this effect. Negatively effective stimulation also significantly increased the RTs (Figures S3H–S3I) and pupil size (Figures S3D–S3E), supporting the hypothesis that the monkeys might have become motivationally influenced. These results favor the hypothesis that the effective microstimulation primarily induced a persistent increase in an anxiety-like internal state.

CN Microstimulation Induced Repetitive Av Choices

Because the induced change in CBR resembling an anxiety-like state tended to be long-lasting and persistent, it was possible that such a persistent negative state might continuously affect the decision-making patterns across trials. We accordingly examined whether the Av choices that we observed could, in addition to being avoidant, be perseverative. Figure 3 shows an example of the extreme repetition of avoidant behavior induced in a session of CN microstimulation. In this session, microstimulation increased the number of Av choices by 13.6% (Figure 3A). Notably, it also induced a repetitive pattern of Av choices (Figure 3B). The maximum number of repetitive Av choices in consecutive trials was seven in the *Stim-off* block but was 23 in the *Stim-on* block, even though the same sequences of reward and punishment were offered in the *Stim-off* and *Stim-on* blocks (Figure 3B).

Because an increase in Av choice itself produces an increase in the chance of having repetitive Av choices, we asked whether the observed increase in repetitive Av was significantly larger than that produced by an increase in the number of Av choices by performing random replacement (RR). In the RR procedure, we assumed that each choice was determined independently across trials. To produce the distribution of repetitive Av, we

randomly replaced the choice orders and then counted the number of repetitive Av choices. By performing this procedure 10,000 times, we produced the distribution of the number of repetitive Av choices expected by chance for each number of repetitions (m). As shown in Figure 3C, the observed number of m repetitions of Av choices in the *Stim-on* block exceeded the 95% confidence limit for $m > 3$, suggesting that the observed repetition was significantly more frequent than that is expected from the RR procedure. To summarize the difference between the observed number of repetitions and that of the RR procedure, we averaged z-statistics over m to derive the mean deviation. The mean deviation from the RR procedure was significantly larger than zero ($p < 0.001$, z-test) (Figure 3C).

Regional Differences in Corticostriatal Circuits Responsible for Repetitive Decisions

To test whether such an influence on repetitive Av choices was broadly characteristic of circuits in which microstimulation could induce increases in Av choice, we performed the same analyses for the dataset obtained in our previous study of the pregenual anterior cingulate cortex (pACC), in which we found sites at which microstimulation increased avoidance behavior (Amemori and Graybiel, 2012). In contrast to the results for the CN stimulation, the observed repetition in the *Stim-on* block was predicted by the RR procedure, exemplified by the session shown in Figure S4, suggesting that the observed repetition induced by the pACC stimulation was accounted for by the change in decision frequencies, without the added feature of trial-by-trial extreme repetition.

As a formal analysis of this contrast, we calculated the z-statistics representing the deviation from the RR procedure for each session for each m (Figure S5). The group mean of the mean deviations of the CN sessions was significantly larger than zero ($p < 0.001$, two-tailed t-test) (Figure 4A), suggesting that the CN stimulation increased repetitive Av more frequently than that expected by the RR procedure. Importantly, in some CN experiments, the microstimulation induced abnormally repetitive choices ($p < 0.05$, z-test) without inducing a significant change in decision frequencies (i.e., less than 5% threshold). By contrast, the group mean of the mean deviations of the pACC sessions was not significantly deviated from zero ($p > 0.05$, t-test). Finally, the proportion of sessions in which the numbers of repetitive Av choices were significantly larger than the prediction of the RR procedure was different for the CN and pACC stimulations ($p < 0.001$, Fisher's exact test) (Figure 4B). To test whether the RR procedure could be confirmed by another analysis, we also produced statistically independent samples from the logit models, which produced decision patterns resembling behavioral choices without statistical dependence of sequence (Figure 2C), and this analysis confirmed the results of the RR analysis (Figure S6). These results suggest that the numbers of observed repetitive Av choices did not change with RR in the sessions of pACC stimulation, but repetitive Av choices in the CN stimulation sessions were significantly larger than those predicted by RR analysis. These findings suggest that the pACC and the striatum could have different functions in modifying behavioral flexibility and persistency, as we could detect repetitiveness only in the CN stimulation experiments.

CN Beta Oscillations Represent Decision-Related Variables

Microstimulation of the proposed CN generative circuit sites induced an anxiety-like state with inflexibility and persistency in choice pattern. Given evidence linking emotional

responses and cortical beta oscillations in patients with depression (Lipsman et al., 2014; Merkl et al., 2015), and the proposal that beta-band activity could potentially be implicated in state maintenance (Engel and Fries, 2010), we hypothesized that CN beta oscillations could be correlated with the monkey's subjective valuation reflecting the persistent character of negative decision-making. In searching for the potential neural signals related to the persistent negative state, we therefore analyzed CN activity recorded before, during and after microstimulation experiments.

We analyzed 958 LFP activities recorded in the CN during the *Stim-off* blocks of 112 stimulation experiments and 74 recording-only experiments (STAR Methods). Most of these *Stim-off* LFPs (81%, 780 channels) exhibited beta-band (13–28 Hz) oscillations, and over three quarters of them (93%, 728/780 channels) exhibited spectral peaks within the beta range (Figures S7A–S7B). The majority of the channels with beta oscillations (86%, 667 channels) were deemed to be task-related, as they exhibited significant changes in magnitude between the precue and the cue periods in the *Stim-off* block ($p < 0.05$, two-tailed z-test, Bonferroni corrected). Figure 5A shows an example of the power spectrum recorded from a CN electrode. This channel exhibited a significant difference in power ($p < 0.05$, z-test, Bonferroni corrected) at most frequencies in the beta band between the precue and cue periods in the *Stim-off* block, and was thus defined as being task-related. We tested whether the beta oscillations were modulated by saccadic eye movements. They were not (Figure S7C), suggesting that the beta-band modulation during the cue period was not primarily associated with observable oculomotor movements. From 301 (45%) of those 667 task-related channels (Table S1), we recorded LFPs during the stimulation experiments. Figure 5B shows an example of a channel in which the choice selectivity of beta oscillation exhibited correlation with the negative behavioral effect of the CN microstimulation. During the cue period in the *Stim-off* block, the spectra exhibited significant differences in magnitude between upcoming Ap and Av choices ($p < 0.05$, z-test, Bonferroni corrected). Although stimulation artifacts contaminated the spectra in the *Stim-on* block, the choice selectivity of the spectra was significantly enhanced in the effective *Follow-up* block ($p < 0.05$, z-test), and the enhancement disappeared in the *Recovery* block. Thus, this analysis indicates that modulation of the beta-band activity has an extended time course beyond the time of stimulation.

To quantify how the effective stimulation influenced the task selectivity of total beta-band LFP responses for each block, we performed multidimensional scaling (MDS) to extract their task-dependent features. We constructed beta response matrices of 667 *Stim-off* channels and applied MDS to derive their feature coordinates (STAR Methods) (Figures S7D–S7H). We thus identified five groups of beta response matrices (Figure 5C). The x-axis in Figure 5C (i.e., principal coordinate value, PCV) quantifies the principal feature, and the distance in the MDS map represents the degree of similarity of individual entries in the map. To examine the similarity of each beta response to the behavioral choice pattern, MDS was performed with the Ap and Av behavioral responses. The group of beta responses that had the highest PCVs among the five identified (Figure 5C, red) was located near the Av choice pattern. We called this the N (negative) group of beta responses (Figure 5D, top). The group of beta responses that had the lowest PCV (Figure 5C, blue) was located near the Ap choice pattern; we called this P (positive) group (Figure 5D, bottom). Because the matrices of Ap

and Av choices were at the leftmost and rightmost position in the MDS map, we could thus regard the PCV as a tuning index of Ap-Av choice selectivity for each beta response, derived by an unbiased clustering method.

N-Group Beta-Band Activity Temporally Leads in Differentiating Ap-Av Decisions

The timing of first differentiation of upcoming Av and Ap choices was clearly different for the groups defined by the MDS analysis (Figure 6). To examine these temporal differences, we performed a cumulative onset analysis (STAR Methods) for the beta oscillations in the five groups (Figures 6A and 6B). For each channel, Ap and Av behavioral onsets were defined, respectively, as the onsets of discriminative choices with higher activities for Ap and Av choices. In many (56 of 107) of the N-group beta responses, differential activities of beta oscillation with higher magnitude for Av choices especially occurred with onsets in the early phase of the cue period (Figure 6A, top left). Many (146 of 193) of the P-group beta responses showed differential activities with higher magnitudes for Ap trials (Figure 6A, top right) with onsets in the later phase of the cue period.

For those beta oscillations with higher magnitudes for either Ap or Av choices, we calculated the population means of the time course of their normalized beta power. The population activity of the N-group beta responses showed significant suppression for the Ap choice during the early phase of the cue period ($p < 0.05$, t-test) (Figure 6A, bottom left). The population activity of the P-group beta responses also exhibited suppression for both choices in the early phase, with significantly greater rebound for the Ap choice than for the Av choice during the late phase of the cue period ($p < 0.05$, t-test) (Figure 6A, bottom right). We then examined the distributions of cumulative onsets, deriving them separately for each of the five groups (Figure 6B). The distribution of cumulative onsets of N-group beta responses rose significantly earlier than did those of the other four groups ($p < 0.05$, Kolmogorov-Smirnov test), indicating that the timing of discrimination of Av from Ap choices was earliest for the N group among the five groups. These results demonstrate that the N-group beta responses led the others in time in differentiating upcoming Ap-Av choices and also demonstrated temporal ordering of these oscillatory responses to differentiate upcoming choices.

Within the CN (Figure S7I), N-group beta responses were not frequently observed at the negative effective sites (Figure 6C). It is thus likely that the persistent negative state is supported by a system independent of the putative generative circuit. Around these negative effective sites, we recorded N unit activities (Figure 1G) and P-group beta responses (Figure 6C) more frequently than in other sites. Both N unit activities and P-group beta responses exhibited differential magnitudes for the upcoming choices during the late phase of the cue period (Figures S1H and S7J).

Modulation of Beta-Band Oscillatory Activity Coincided with the Behavioral Effects of CN Microstimulation

In searching for neural correlates of the persistent negative state, we next asked whether the value representation of the CN beta oscillation was indeed modulated in the *Follow-up* block. We applied the MDS clustering procedure to the beta responses for each block of

stimulation sessions in order to examine whether and how the influence of stimulation on the beta response in the effective sessions is different from that in the non-effective sessions. For this purpose, we selected the beta responses that could be recorded continuously from the *Stim-off* block all the way through to the *Recovery* block (Table S1). We selected 84 channels in the effective sessions and 90 channels in the non-effective sessions, as they were stably recorded. We performed MDS to characterize the beta responses for each block (Figures 7A and 7B), and used the PCV of each channel to quantify the choice selectivity of the beta responses. The group mean PCV of the 84 channels in the effective sessions was significantly larger in the *Follow-up* blocks than in the *Stim-off* blocks ($p < 0.001$, t-test) (Figure 7A), indicating that the population of beta responses represented negative motivational variables specifically in the *Follow-up* blocks. No such stimulation-induced changes occurred for the channels recorded in the non-effective sessions. The close parallel between the persistent changes in the mean of the beta responses and the sizes of increase in Av decisions support a link between beta oscillation and the persistent anxiety-like state induced by CN microstimulation.

As the number of N-group beta responses significantly increased in the effective *Follow-up* block ($p < 0.001$, Fisher's exact test) (Figure 7C), it is possible that there were some channels that did not show choice selectivity in the *Stim-off* block but exhibited the selectivity in the effective *Follow-up* block. To address this possibility, we performed the MDS classification for *Stim-off*, *Follow-up* and *Recovery* blocks for effective and non-effective sessions. We designated the 32 channels that were classified as N-group beta responses in the *Follow-up* blocks as N-f channels, and examined how they were classified in the *Stim-off* and *Recovery* blocks (Figure 7B). Twenty-five N-f channels (78%) in the *Stim-off* block and 22 N-f channels (69%) in the *Recovery* block were not classified as N-group beta responses. In the effective *Follow-up* block, abnormal beta oscillation could thus newly emerge in the *Follow-up* block and disappear in the *Recovery* block. The mean power spectra of N-f channels exhibited a significant increase in choice selectivity specifically in the low beta band ($p < 0.05$, z-test) (Figure S8A), whereas the mean power spectra of the other channels did not (Figure S8B). The low-beta responses selective for the upcoming choice appeared in the early phase of the cue period, and the selectivity in the early phase was enhanced in the *Follow-up* block (Figures S8C and S8D). Therefore, in a subset of CN channels (i.e., N-f channels), modulation of beta oscillation was tightly correlated with the persistent negative state throughout a series of blocks in the negative effective sessions.

Modulation of Beta Responses Encodes Previous Av Choices

The critical functional requirement for a repetitive choice pattern is a neural signal encoding the choice in the preceding trial. We thus focused on the neural activity during the intertrial interval, specifically when we observed excessive repetition of Av choices (Figure 3). If the beta-band modulations were involved in, or were a correlate of, a repetitive choice pattern, then during the time in which the monkeys repetitively made the same choices, beta oscillations during the precue period could encode the previous choice. We examined the LFPs of 113 channels in sessions in which CN microstimulation induced repetitive choice patterns significantly more frequently than the RR predictions ($p < 0.05$, z-test). For these channels, we focused on the beta oscillatory activities during the precue period and tested

whether they showed differential activities for the preceding choices. The precue power spectrum of 23 channels (20%) exhibited significant differences in magnitude between the preceding Ap and Av choices in one of the three blocks. In 16 channels, the precue spectrum exhibited significant elevation in the beta range if Av choice occurred in the preceding trial ($p < 0.05$, z-test), whereas the spectrum in seven channels showed significant elevation for the preceding Ap choices. We then asked whether effective microstimulation modulated the beta response profiles during the precue periods. We derived a precue Av-Ap tuning index by subtracting the precue spectrum for the preceding Ap choices from that for the preceding Av choices (i.e., selectivity for preceding Av choice). The normalized group mean of the Av-Ap tuning indices significantly increased in the *Stim-on* and *Follow-up* blocks compared to that in the *Stim-off* block ($p < 0.05$, t-test) (Figure 8A). These results indicate that the selectivity of the beta response for the preceding Av choice was enhanced for these 16 channels, especially when the monkeys showed abnormal repetition of Av choices. Seven channels exhibited significant elevation of beta magnitude if the preceding trial had Ap choices, but there was no clear correlation with the repetitive choice pattern (Figure 8B).

These results suggest that persistent beta oscillatory activity recorded on a subset of CN channels exhibited selectivity for the preceding Av choice, and that the effective microstimulation that induced excessive behavioral repetition further enhanced the selectivity. We could not determine whether the relationship between the beta-band modulation and the repetitive choice behavior was part of a causal mechanism, or was indirect and therefore not causal; but we have demonstrated that the beta activity was correlated with the memory of the previous choice up to the time when the monkey was required to make the next decision. As the selectivity for the preceding Av choice in the precue period was specifically enhanced when the subject repeated Av choices, the persistent beta activity could be a correlate of a function bridging the choice patterns in preceding and upcoming Av choices.

DISCUSSION

Our findings in non-human primates point to local CN sites as potential generative circuits that are involved in producing a mood-like, persistent state, one influencing the repetitiveness of negative decision-making. Human imaging studies have demonstrated that the CN exhibits abnormal activity in depressed individuals (Price and Drevets, 2012). In non-human primates, CN stimulation has been shown to facilitate affect learning (Williams and Eskandar, 2006) and saccadic eye movements (Nakamura and Hikosaka, 2006), to induce hyperactive behavior (Worbe et al., 2011) and to bias choices of movement directions (Ding and Gold, 2012). We found that the stimulation of CN local circuit sites generated persistent states of negative valuation under motivationally challenging Ap-Av conflict, suggesting that the CN could be an origin of circuits producing irrationally persistent value judgments that in turn induce repetitive negative valuation. By contrast, new analysis of data collected during pACC recording (Amemori and Graybiel, 2012) indicated that pACC microstimulation did not induce abnormally persistent choice patterns, despite inducing avoidance behavior.

Previous reports have emphasized positive aspects of CN function, as it is involved in facilitating reward-seeking behaviors in primates (Kim and Hikosaka, 2013; Nakamura and Hikosaka, 2006; Williams and Eskandar, 2006), but we found more negative sites than positive sites. In the decision matrix that we used to detect the change in decision frequencies, the area of Ap was larger than that of Av in the baseline *Stim-off* block. This baseline bias was self-determined by the monkeys, and because of the higher Ap baseline, changes from Ap to Av might have been easier to observe than those from Av to Ap might have. Another possible reason for the large number of negative sites is that the localized CN microstimulation induced a facilitation of an avoidance behavior that was neglected in previous studies in primates, perhaps because negative effects in the previous reports were regarded as a suppression of reward-seeking behavior. Further, in the Ap-Av task that we used, we could also detect facilitation of an avoidance behavior. Such explicit examination of an active avoidance in conflict behavior has not been reported before in non-human primates. Despite these alternatives, there remains the possibility, favored here, that there are, in fact, more negative than positive sites.

Potential Link between Excessive Repetitive Decisions and CN Beta Oscillation

In both rodents and non-human primates, repetitive, stereotypic behaviors induced by psychomotor stimulants have been found to alter gene expression in the striatum (Canales and Graybiel, 2000; Saka et al., 2004), and optogenetic interference of an orbitofrontal corticostriatal circuit has been found to causally regulate compulsive, repetitive behavior (Ahmari et al., 2013; Burguiere et al., 2013). This evidence accords with a large literature implicating the orbitofrontal cortex and its serotonergic input in the control of behavioral flexibility (Clarke et al., 2004). Electrical stimulation of the primate striatum is also known to induce such stereotyped behaviors (Worbe et al., 2011). Our experiments provided repeatable experimental evidence to show that the primate striatum is causally involved in the induction of abnormally repetitive choices, often accompanied by a persistent anxiety-like state. Quantitative comparisons of repeated choice patterns between the pACC and CN stimulation experiments further support the conclusion that the CN is a major source of the abnormal repetitive choices in corticostriatal circuitry.

Studies in humans have suggested that the modulation of beta oscillations recorded in the ventromedial prefrontal cortex of patients with mood disorders is associated with the emotional responses of the subjects (Lipsman et al., 2014; Merkl et al., 2015). We focused on the striatum, and in particular the CN, which is reported to show abnormal activities in human OCD patients (Price and Drevets, 2012), and we examined whether and how the CN beta oscillations could be modulated in parallel with the persistent negative state. We found an enhancement of beta-band magnitude after Av choices stretching through the precue period. Based on the view that beta-band oscillatory activity could be related to maintenance of the current state or status quo, the enhancement of striatal beta oscillation could stabilize current behavioral planning by reducing the influences of other alternative actions (Leventhal et al., 2012). Our findings did not provide causal evidence for the direct role of beta-band activity. However, by this view of stabilization as a function of beta activity, the enhanced Av tuning of beta oscillations after Av choices could reflect the stabilization of Av

choice behavior, leading to facilitation of repetitive choices by bridging between previous and current choices.

Neural Mechanism of Persistent Pessimistic State Induced by the CN Microstimulation

The persistent negative state induced by CN microstimulation was correlated with the modulation of CN beta-band activity observed outside of the proposed generative circuit sites for acute effects (Figure 6C). To account for this observation, we suggest as a working hypothesis that the generative circuit, in part, includes a striatonigral projection circuit (Figure S8E). By this view, the stimulation of the generative circuit sites could have suppressed dopamine (DA) or other aminergic systems. Induced DA suppression could have acutely produced an increase in Av choice with the changes in cost-benefit integration, and could subsequently have induced a long-term change in reactivity of striatal neural circuits, specifically at the projection sites of the affected DA circuit. It is therefore reasonable to suggest that the persistent change in neural signal was generated independent of the local generative circuit, given our observation that the modulation of N-group beta responses was observed outside of the negative effective sites.

According to this possibility, the persistent negative state induced by the stimulation of the proposed generative circuit sites could be related to long-term changes in neuronal reactivity at the projection sites of the acutely suppressed DA system. It is known that striatal beta oscillatory activity is strengthened in DA-depleted states (Goldberg et al., 2004), as observed in Parkinson’s disease (Jenkinson and Brown, 2011). Relevant to our findings, some patients with Parkinson’s disease have been reported to show impairment in conflict decision-making (Frank et al., 2005) that could be regulated by deep brain stimulation normalizing beta oscillations in the basal ganglia (Cavanagh et al., 2011). One possible mechanism of the strengthened beta oscillation is an imbalance between cholinergic and dopaminergic activities (Aosaki et al., 2010), induced specifically at the projection sites of the affected DA circuit. The local suppression of striatal DA may consequently have strengthened striatal cholinergic activity, which is considered to enhance the beta oscillation (McCarthy et al., 2011).

It is known that the striatum contains focal regions called striosomes, and that in rodents, these have been shown to project directly to subsets of DA-containing neurons of the substantia nigra, pars compacta (Crittenden et al., 2016; Fujiyama et al., 2011). Striatonigral afferents in rodents affect the activity of DA-containing neurons in the substantia nigra (Brazhnik et al., 2008). Moreover, striosomes project into the pallido-habenular circuit that can affect both DA and serotonin systems of the midbrain (Rajakumar et al., 1993). Together, these systems could control decision-making based on rewarding and aversive stimuli (Hikosaka, 2010). Striosomes receive input from the pACC and the caudal orbitofrontal cortex (Eblen and Graybiel, 1995), both associated with the control of repetitive vs. flexible behavior (Burguiere et al., 2013; Clarke et al., 2008). It is possible that the CN generative circuit sites that we identified here correspond to striosomes in the anteromedial striatum, a region in which experimental work in rodents has been shown to be a critical node in corticostriatal decision-making circuits (Friedman et al., 2017; Friedman et al., 2015).

We used Ap-Av choices as a proxy for measuring the internal states of the monkeys indicating positive (optimistic) or negative (pessimistic) evaluation of future options. We were unable to analyze the connections of the effective sites of microstimulation, nor determine whether they were in striosome or matrix compartment of the striatum. However, our unit recording at negative effective sites suggested a close relationship between cellular spike responses and the evoked pessimistic valuation. The surprisingly strong changes in evaluative decision-making that we have found by sub-cortical microstimulation, and the specificity of induction of long-lasting states of negative evaluation associated with selective beta-band patterning during decision-making, point to the striatum as a potentially powerful driver for the induction of mood changes including excessive and persistent pessimism.

STAR METHODS

CONTACT FOR REAGENT AND RESOURCE SHARING

Further information and requests for resources and reagents should be directed to and will be fulfilled by the Lead Contact, Ann M. Graybiel (graybiel@mit.edu).

EXPERIMENTAL MODEL AND SUBJECT DETAILS

Two *Macaca mulatta* monkeys (S, 7.5 kg, ~6 year old female; P, 6.3 kg, ~5 year old female) were studied in experiments conducted in accordance with the Guide for Care and Use of Laboratory Animals of United States National Research Council. All procedures were approved by the Committee on Animal Care of the Massachusetts Institute of Technology.

METHOD DETAILS

Surgical Procedures—Before training, the monkeys were habituated to sitting in a monkey chair. For the training, a custom-made non-invasive head-fixation device (Amemori et al., 2015b) was made for each monkey. After the monkeys learned to perform the task, we mounted a recording chamber on the cranium during sterile surgery performed under deep anesthesia. Prior to the chamber implant, structural magnetic resonance images (MRIs, T1 and T2 weighted images, 350 mm resolution; 3.0 Tesla; Siemens) were obtained to aid in placement of the recording chamber. During surgery, anesthesia was induced by intramuscular ketamine (10 mg/kg), given with atropine (0.05 mg/kg), followed by inhalation of 1–2.5% sevoflurane with O_2. Ceramic screws and bone cement were used to secure the recording chambers. For all surgeries, the monkeys were maintained on analgesics postoperatively, and prophylactic antibiotics were injected intramuscularly both on the day of surgery and daily thereafter for 1 week.

Task Procedures—The monkeys were trained to perform the Ap-Av task (Figure 1A). The task has been previously described in detail (Amemori et al., 2015a; Amemori and Graybiel, 2012); a summary is provided here. In the task, a white central fixation spot and a gray rectangular frame appeared on a computer screen in front of the monkey at the initiation of the task. When the monkey placed its hand on a designated start position, an infrared photo beam sensor detected the placement, inducing the rectangular frame to turn white. The monkey was required to hold its hand in the start position for 2 s and to fixate at the central fixation spot (fixation period). After this fixation period, a compound visual cue,

consisting of abutting red and yellow horizontal bars, appeared within the rectangle, with the fixation point still present. The length of the red bar signaled the offered amount of liquefied food to be offered (0.1 to 2.0 ml). The length of the yellow bar signaled the pressure of the airpuff to be offered (0 to 60 psi). The cues remained on for 1.5 s (cue period). If the monkey released the contact during this time (a commission error), the trial was terminated, and an airpuff corresponding in strength to that indicated by the length of the yellow bar was delivered to the monkey's face. After the monkey maintained fixation during this cue period, two target cues (a white cross and a white square) appeared above and below the cue. At the same time, a cursor (white circle), whose vertical location could be controlled by a joystick held by the monkey, appeared at the center of the screen. The monkey was required to report its decision by using the joystick to move the cursor toward one of the two targets within 3 s (response period). The locations of the targets were alternated randomly. If the monkey did not respond within the allotted 3-s response period, the trial was registered as an omission error, and an airpuff, in the strength indicated by the yellow bar, was delivered. When the monkey chose the square target, a sound signaling Av was played, and a minimum and constant amount of reward (liquefied food, 0.1 ml) was delivered, but no airpuff. If the monkey chose the cross target, a sound signaling Ap was played, an airpuff whose pressure was indicated by the yellow bar was delivered to the monkey's face for 800 ms, and liquefied food, in an amount signaled by the red bar, was then delivered 1 s later for 1.5 s. After each trial, a 5–8 s intertrial interval (ITI) followed. The precue period was defined as the 2-s window before the cue onset, consisting of the last 2 s of the ITI and the fixation period. No distinctive differences in features of the beta oscillations for the ITI and the fixation period were observed. The amount of reward was controlled by a computer and a pump attached to the food tube (L/S Masterflex, Cole-Parmer). The compressed air for the airpuff was generated by an air compressor (20-A, Silent Air) and was controlled by a computer and an E/P transducer (900-EIA, Control Air).

Electrode Implant, Microstimulation and Electrophysiological Recordings— After the placement of the recording chamber, a plastic grid was placed in the chamber. The grid had openings spaced at 1-mm intervals to serve as guides allowing parallel microelectrode penetrations. After this grid placement, another set of MRIs was taken to allow subsequent identification of the electrode tracks. Then, in a second sterile surgery under conditions of surgical anesthesia, the skull overlying the targeted regions was removed. After recovery, in a third sterile surgery, sets of platinum-iridium electrodes (impedance, 0.1–1.0 MΩ; FHC) were implanted for chronic recording (Feingold et al., 2012). All electrodes were held by custom-made micromanipulators affixed to the grid. For the implant in monkey S, 43 electrodes were implanted simultaneously into the neocortex, 12 in the dorsolateral prefrontal cortex (dlPFC) and 19 in the anterior cingulate cortex (ACC), and 15 in the CN of the right hemisphere. For the implant in monkey P, 66 electrodes were implanted in the neocortex (6 in the dlPFC, 12 in the ACC, and 18 in the orbitofrontal and ventromedial prefrontal cortices) and subcortical regions (18 in the CN, and 9 in other regions) in the left hemisphere. The location of each electrode was estimated by the MRI and neuronal properties recorded by the electrodes during experimental procedures. After the experiments, all electrode locations were confirmed by histological reconstruction of the electrode tracks. Here we describe findings for the striatal electrodes; results obtained from

the neocortical targets are described elsewhere (Amemori et al., 2015a; Amemori and Graybiel, 2012). For stimulation experiments, one lead of the stimulator was connected to the ground, and cathode-leading biphasic pulses were applied to the microelectrode. In the recording-only experiments, recordings were made while the monkeys performed each of the two different (Ap-Av and Ap-Ap) tasks in alternating blocks of 150 trials (Figure S1B). In the Ap-Ap experiments, lengths of red and yellow bars were associated with the amount of offered reward, and the reward amount was used to derive the decision (Amemori et al., 2015a). After the stimulation experiments of all electrodes, the electrodes were advanced simultaneously. Before re-starting the stimulation experiments, we performed the recording-only experiment so that we could record LFPs from every stimulation site.

Size of Change in Decision Frequencies Induced by the Microstimulation—The size of change in Ap-Av decisions was calculated in the decision matrix (Figures 1D and 1E) as follows. The choice in each trial was convolved with a 30-by-30 point square-smoothing window. After this spatial smoothing, each choice datum was stacked at each point in the 100-by-100 point decision matrix. We then calculated decision statistics such as the mean and t-statistics for each point using the stacked choice data. We used Fisher's exact test to detect statistically significant differences between choices in two different blocks with a threshold of $p < 0.05$ at each point. The change in decision frequencies between the *Stim-off* and *Stim-on* blocks was then represented by the total fraction of points in the decision matrix that showed a significant increase in Av (%ΔAv) plus the fraction that showed a significant increase in Ap (%ΔAp).

Firstly, to evaluate whether the microstimulation significantly affected the choices or not, we compared the total change (i.e., %ΔAv + %ΔAp) in each stimulation session with those in the recording-only sessions. In the 74 recording-only sessions, the block of Ap-Ap task separated two blocks of Ap-Av tasks. The distribution of the total change in choice between two Ap-Av blocks showed stability in the recording-only sessions (Figure S1B). We set a total change of 5% as the threshold to discriminate effective and non-effective stimulation sessions. In the 71 recording-only sessions (96.2%), the size of the total change, %ΔAv + %ΔAp, was less than the discriminating threshold, and then the false positive rate to misclassify non-effective as effective by this criterion was less than 0.05.

Secondly, we examined the plausibility of choosing the 30-by-30 point square-smoothing window. Using the logit model derived from the mean choice pattern, we produced two groups of 200 statistically independent choices, and calculated the difference between the two groups (Figure S1C). With the 5% discriminating threshold, the false positive rate to misclassify those as significantly different was 2.2%. Even with the 40-by-40 point square-smoothing window, the false positive rate was less than 5%. We thus concluded that the choice of 30-by-30 point square-smoothing window is plausible.

Lastly, we confirmed the stability in the 11 no-stimulation experiments (Figure S1D). For each no-stimulation experiment with saline infusion but without microstimulation, we separated each no-stimulation session into three blocks of 200 trials, and intramuscularly infused saline (0.3 ml) between the first and second blocks. The upper bound of the 95% confidence interval of the change in decision frequencies between the first and second *Stim-*

off blocks was 1.5%, and that between the first and third blocks was 4.1 %, both below the discrimination threshold. These results, acquired between different stimulation experiments, indicated the Ap-Av choice behavior was stable in the absence of microstimulation. This infusion informed the monkey about the time of the block change, but it did not affect the decision pattern.

Among 112 stimulation experiments, we thus defined 41 sessions as effective by this discrimination threshold (Figure S1E). We used the difference in negative and positive effects (i.e., %ΔAv − %ΔAp) to show the direction of the stimulation effect. In most (38 of 41) stimulation experiments, the effects were an increase in either Ap or Av choices. After one positive and 18 negative sessions in which the choice pattern did not recover in the *Follow-up* block, we then continued to perform a no-stimulation experiment (*Extended session*) until the choice pattern returned to baseline levels (Figures 2A and 2B). These *Stim-off* sessions were separated into blocks of 200–250 trials, and the choice in each block was compared with the *Stim-off* block in the stimulation session. The first block in which the increase in Av became less than the discrimination threshold was designated as the *Recovery* block. In five negative sessions, the choice pattern recovered to baseline levels in the *Follow-up* block. To derive the CBR and PCV for these sessions, we used the data in the *Follow-up* block for those in the *Recovery* block.

Histological Identification of Electrode Tracks—Microelectrodes were kept in place during perfusion. The monkeys were deeply anaesthetized with an overdose of sodium pentobarbital and were perfused with 0.9% saline followed by 4% paraformaldehyde in 0.1 M phosphate buffered saline (PBS). Brains were kept in 4% paraformaldehyde for 3 days, and then electrodes were withdrawn. Then brains were blocked and stored in 25% glycerol in 0.1% sodium azide (438456; Sigma) in 0.1M phosphate buffer (PB) at 4°C until being frozen in dry ice on a sliding microtome and cut into 40-μm coronal sections. Sections were stored in 0.1% sodium azide in 0.1M PB. To identify the electrode tracks, some striatal sections were immunostained for glial fibrillary acidic protein (GFAP) immunofluorescence, and the other sections were stained with cresylecht violet for Nissl substance. Sections were examined microscopically and then imaged with an automatized slide scanner (TissueFAXS whole slide scanner; TissueGnostics) fitted with 10× objectives. For GFAP immunofluorescence staining, sections were rinsed 3 times for 2 min in 0.01M PBS containing 0.2% Triton X-100 (Tx) (T8787; Sigma-Aldrich) and then were pre-treated with 3% H_2O_2 in PBS-Tx for 10 min. Sections were rinsed 3 times for 2 min in PBS-Tx, and were incubated in tyramide signal amplification (TSA) blocking reagent (FP1012; PerkinElmer) for 60 min. Then the sections were incubated with primary antibody solutions containing rabbit anti-GFAP (z0334; DAKO) in TSA blocking reagent in PBS-Tx for 24 hr at 4°C. After primary incubation, the sections were rinsed 3 times for 2 min in PBS-Tx, and then were incubated for 2 hr in secondary antibody solution containing goat anti-rabbit Alexa Fluor 488 [1:300] (A11034; Life Technologies) in TSA blocking reagent in PBS-Tx. After 3 rinses for 2 min each in 0.1M PB, sections were mounted onto glass slides and coverslipped with ProLong Gold antifade reagent (P36930; Life Technologies).

Econometric Modeling—If there are two options respectively associated with the cross and square targets, the probability of choosing the cross target can generally be written as $p_{AP} = 1/(1 + \exp(-(U_{AP} - U_{AV})))$, where U_{AP} and U_{AV} are the utility of each option (Train, 2003). In the Ap-Av task, the function $f = U_{AP} - U_{AV}$ was approximated by the first-order linear model that had the lowest Bayesian information criterion (BIC) (Amemori and Graybiel, 2012). We thus parameterized the function $U_{AP} - U_{AV}$ as $f(x, y) = ax + by + c$, where x was the length of red bar, y was the length of yellow bar, and a, b, and c were the coefficients determined by generalized linear regression fitted to the behavioral choices. We modeled each utility as $U_{AP} = ax + by$ and $U_{AV} = -c$. The expected value of the outcome or "chosen value" was calculated as ($ChV = p_{AP}U_{AP} + (1 - p_{AP})U_{AV}$) (Figure 2C). Cost-benefit ratio ($CBR = -b / a$) was defined by the ratio of the sensitivities to benefit (reward) and cost (airpuff). The slope of the decision boundary ($-a / b$) is the reciprocal of the CBR.

Normalization Procedure for Standard Decision Boundary—For analyses of averaged unit and beta responses (Figures 5D, S1F, S1G, S1H and S7J) and behavioral performances (Figures 1B and 1C) in different sessions, we needed to map the behavioral responses to a standard decision matrix, so that we could compare data across different daily sessions and across different blocks. We performed a normalization procedure by transforming the behavioral data before we accumulated or compared them across sessions (Figure S2A). For the dataset that produced decision boundary $ax + by + c = 0$, we applied the procedure described previously (Amemori and Graybiel, 2012) to the dataset in order to have the standard decision boundary $a_0x + b_0y + c_0 = 0$. We set the standard decision boundary to pass through (5, 0) and (50, 100). For every datum that was to the left of the decision boundary, we resized x as $x' = xX_a / X_b$, where $X_a = -(c + by) / a$ and $X_b = -(c_0 + b_0y) / a_0$. For a datum that was to the right of the decision boundary, we resized x as $x' = 100 - (100 - x)X''_a / X''_b$, where $X''_a = 100 + (c + by) / a$ and $X''_b = 100 + (c_0 + b_0y) / a_0$. With this procedure, the decision boundary derived from the transformed data corresponded to the standard decision boundary. To derive the gradual change induced by the stimulation (Figure 2D), we derived the transformation procedure based on the choice pattern in the *Stim-off* block, and the same procedure was applied to the choices in the *Stim-on* block so that we could compare the choice pattern in two blocks. We confirmed that without this procedure, all the conclusions derived from the subsequent analyses did not change.

Procedures for Control Experiments

Control Experiment 1 (diazepam administration).: Control Experiment 1 was conducted at four negative effective sites to determine how an anxiolytic treatment affects the persistent negative states produced by CN microstimulation (Figures 2F and S2B). Two monkeys performed 600 trials of the Ap-Av task during a single session divided into three blocks: *Stim-off* (200 trials), *Stim-on* (200 trials), and *Stim-on* after drug administration (200 trials). Microstimulation (150 μA) was applied during the second and third blocks, and diazepam (a benzodiazepine $GABA_A$ agonist, 0.25 mg/kg, IM) was administered as a single intramuscular injection during the trial interval between the second and third blocks. The concentration of diazepam was chosen according to dose-response curves calculated previously (Amemori and Graybiel, 2012). Each block lasted ~55–60 min.

Control Experiment 2 (rCMA stimulation).: Control Experiment 2 was conducted to exclude a potential influence of stimulation-induced movement (Figure S2C). In this experiment, we applied microstimulation (150 mA) in the dorsal bank of the cingulate sulcus around the border between pre-supplementary motor area and rostral cingulate motor area (rCMA) to induce left arm movement (Luppino et al., 1991). We confirmed that the actual induction of an arm movement was not sufficient to change the decision between the *Stim-off* and *Stim-on* blocks (250 trials for each block). Irritations induced by visible or invisible movements induced by the stimulation could also be considered as a potential reason to change the decisions of the monkeys.

Control Experiment 3 (eye movement monitoring).: Control Experiment 3 was conducted at three negative effective sites to confirm that the microstimulation did not induce eye movements (Watanabe and Munoz, 2010) or autonomic responses indicative of pain (Figures S3A–S3G). The two monkeys were trained further to perform a fixation task in which ocular fixation was required. At the start of the task, a circular fixation cue appeared at the center of a black screen in front of the monkey. When the monkey's gaze acquired the fixation circle, a square cue replaced the circular cue. Then the monkey was required to maintain its gaze within a fixation window of 5° for 3 s. Liquid food reward was delivered after successful fixation. Microstimulation, generated by the stimulator (Master-8, A.M.P.I.) and isolator (A365, WPI), started from the appearance of the square cue and lasted for 1 s. The stimulation induced no eye movements (Figures S3A–S3C). The parameters for microstimulation were the same as those used during the cue period in the Ap-Av task. After 100–200 trials in the no-stimulation (*Stim-off*) block, a block of stimulation trials (200–300 trials) followed. The pupil size was normalized by the mean size in the 3-s fixation period of the *Stim-off* trials before being averaged. Skin conductance (μS) monitored from the monkey's palm was normalized by the value averaged over the 10-s period before the task starts. For comparison, an unexpected airpuff was delivered out of the task. In two of the three experiments, we detected a significantly larger pupil size induced by the stimulation ($p < 0.05$) (Figures S3D and S3E). The change in skin conductance was compared to that induced by an airpuff (~15 psi) to the monkey's face. In all of the three experiments, we could not detect a change in skin conductance induced solely by microstimulation of the effective site, whereas we could detect a significant increase in the skin conductance induced by the direct delivery of the airpuff (Figures S3F and S3G). The lack of change in the skin conductance upon striatal microstimulation in our experiments suggests that the perceptual experience induced by the stimulation was small compared to that induced by an airpuff delivery.

Spike and LFP Recording—We performed 112 stimulation experiments during which we recorded spike and LFP activity in the CN from the electrodes that were not used for the stimulation. Additionally, we recorded LFPs without stimulation in 74 sessions. The numbers of these different recordings are summarized in Table S1. LFPs were originally recorded with respect to a skull reference, but in offline analysis, we used local average referencing. The recording and task-control system consisted of five networked computers and other peripheral equipment. Eye positions were monitored by an infrared eye-movement camera system (Eyelink 1000; SR Research). Two computers controlled the behavioral task

based on a CORTEX system developed by the National Institute of Mental Health. For recording, a digital data acquisition system (Digital Lynx; Neuralynx) collected all signals and task event markers. Signals from the electrodes were amplified and stored by the Digital Lynx system. Data were further classified into single-unit activities using Offline Sorter (Plexon), and unit and LFP data were analyzed using MATLAB (MathWorks). Importantly, the electrode selected for the stimulation was one from which we found single units with task-related activity, so that their activity could be compared to the effects of stimulation. This procedure was intended to reduce the chance that stimulation effects were related to fibers of passage, and although we could not preclude such effects, we could make sure that the sites of stimulation had units related to the decision-making task. After the completion of the stimulation delivered at the selected electrode in a given experimental series, we lowered all of the implanted electrodes at once by ~500 μm to search for the next sites. Therefore, the distances among all electrodes were kept as they had been.

Beta-Band LFP Responses—The timing of the stimulation sent from the stimulator was recorded along with the LFPs in each channel. Electrical stimulation artifacts were removed from the raw 32 kHz-sampled files by linear interpolation between the time points 50 μs and 1.5 ms after the onset of the stimulation trigger pulse. In some instances, in which the recording electrode was extremely close to the stimulating electrode, the amplifier took longer to settle into a usable range than the interval between stimulation pulses, producing a distorted signal throughout the stimulation period; no attempt was made to remove stimulation artifacts from such channels. To reduce external noise and volume-conducted neural potentials, a local average reference signal was computed by averaging the signals from all electrodes within each local electrode group (Figure S1A): the reference was calculated by averaging the signals in a subregion of the CN. Electrodes were grouped based on their anterior-posterior positions, and the averaged LFPs of each group were used as the reference for each electrode in the group.

To reduce file size and computation time, each channel was down-sampled by a factor of 32 as follows. The signal was low-pass filtered twice, in forward time and reverse time, with a 4th order Butterworth filter having a cutoff frequency equal to 0.45 times the target sampling rate (1 kHz), and every 32nd sample was used. Beta-band power as a function of time was calculated by band-pass filtering the signal once in forward time with a 4th order Butterworth filter having a pass band of 13 to 28 Hz. Each filtered sample value was then squared and the time series was smoothed with Hanning kernel 77 ms wide at half-height (i.e., one cycle of the lowest frequency in the pass band).

All spectral analysis was performed by the multitaper method (Bokil et al., 2010), and the DC component in each time window was removed before applying tapers. Four tapers were used, each with a time-half-bandwidth product (“NW”) of 3. For precue period, the window width was 3.95 s, and for cue period, it was 1.5 s. Spectrograms (Figure 5A) were computed using a 0.75-s window. To highlight small power differences, an analytic pink noise spectrum of the form, $p = af^b$, was used as a baseline. The parameters a and b were fitted separately for each channel by taking the logarithms of power and frequency, and then fitting the straight line, $y = \log a + b \log f$, to the data points, $y = \log p$. If the power spectrum of the precue period (the 4-s period before the cue onset) or that of the cue period was

significantly greater than the analytic pink noise spectrum in the beta frequency band (13–28 Hz; $p < 0.05$, two-tailed z-test, Bonferroni corrected for the number of independent frequency points, which we estimated as the width of the beta band divided by the smoothing bandwidth of the taper set), we defined that channel as exhibiting beta oscillations (Table S1). Among 958 LFPs recorded in the *Stim-off* block, 780 channels (80%) exhibited beta oscillations. Among them, the averaged power spectrum of the cue period was significantly different ($p < 0.05$, two-tailed z-test, Bonferroni corrected as above) from that of the precue period in 86 % of the channels (667), and these LFPs were defined as task-related beta responses. Baseline-subtracted power spectra were calculated by subtracting the fitted pink-noise spectrum from the spectrum of each task period.

Classification to Derive N, P and the Other Groups of Beta-band Oscillatory Activity—In Figures S7D–S7H, we show the procedure of the MDS-based clustering to derive 5 groups. First, for 667 channels, we performed band-pass filtering of the task-related LFPs and derived the time course of beta-band power for each trial (Figure S7D). To classify these beta responses, we focused on the cue-period beta power in the *Stim-off* block, avoiding the stimulation artifact present in the *Stim-on* blocks. The beta power magnitudes were mapped to an 8-by-8 decision matrix and were averaged over all trials to produce a beta response matrix (Figure S7E). Based on the similarities among these beta responses, we classified them as follows. We used the cross-correlation r_{ij} between each pair of beta response matrices i and j as a similarity index, which we then converted to a correlation distance matrix $D = [d_{ij}]$ where $d_{ij} = 1 - r_{ij}$. With the correlation distance matrix of 667 beta responses (Figure S7F), we performed MDS to derive feature coordinates that maximally differentiated dissimilar responses (Figure S7G). The eigenvalue of each dimension (λ_d) represents the magnitude of the explanatory power of dimension d (Figure S7H). The adequacy of the 4-dimensional representation was estimated by the formula, $\left(\sum_{d=1}^{4} \lambda_d^2\right) / \left(\sum_{d=1}^{667} \lambda_d^2\right)$, which was over 80%. We thus used the corresponding four dimensions to represent the beta response of each channel for the following analyses.

The dataset in the 4-dimensional space was fitted with a Gaussian mixture distribution model (*fitgmdist* function of MATLAB using expectation maximization algorithm; maximum iterations allowed: 10^5; diagonal convergence type), where the optimum number of clusters was selected by BIC to be five (Figure S7H). For each channel, we designated the group that gave the highest posterior probability. Beta responses were projected onto the first two dimensions of the MDS (the MDS map), as shown in Figure 5C. A. U. in the MDS map represents the distance produced by the MDS procedure. Having classified each channel using the 8-by-8 matrix, we recalculated averaged beta responses by a 25-by-25 matrix for purposes of illustration in the figures. Subsequent analyses were done on the original 8-by-8 matrices. In the MDS map, we derived the positions of Ap and Av choices by the same MDS procedure with the combination of 667 *Stim-off* cue-period beta response matrices and the matrix of choice pattern.

Spatial Correlation between Negative Effective Site and Cellular Responses—We performed unit and LFP recordings in the recording-only sessions immediately after we changed the spatial configuration of the implanted electrodes, prior to the stimulation

experiments (Figures 1G and 6C). With the cue-period activities of these 526 spike recordings, we performed correlation analyses between the upcoming Ap-Av choices and the cue-period activities ($p < 0.05$, Pearson's correlation coefficients). The cue-period activities of 82 units showed a significant positive correlation with the upcoming Ap choice, and those were classified as P units (Figure S1F). The cue-period activities of 42 units showed a significant positive correlation with the upcoming Av choice, and those were classified as N units (Figure S1G). To examine the spatial structure of neural activity around the negative effective sites, we examined the distribution of unit and beta responses around 25 negative effective sites. Fifteen N units were recorded within the 1-mm bin around the negative sites, and the spike density function of these units is shown in Figure S1H.

Cumulative Onset Analyses for the Beta Responses—As shown in the upper panels of Figure 6A, we derived the onset of the time of discriminating upcoming Ap and Av choices during the cue period. We calculated the power in the beta band (13–28 Hz) at each time point, smoothed it with a moving average filter (window = 100 ms), and computed p-levels and z-statistics by a two-sided Wilcoxon rank sum test (*ranksum* function of MATLAB) for each time point. The z-statistics are shown in pseudocolour raster plots in the upper plot of each panel, with shades of blue and red indicating, respectively, higher power for upcoming Ap and Av decisions. We defined the onset of choice discrimination as the earliest time at which the Wilcoxon test returned $p < 0.05$ consecutively for more than 100 ms. Onsets could be of the Ap type, indicating higher power on Ap trials, or the Av type, indicating higher power on Av trials. Channels with Av onsets are shown in the order of onset times in the lower part of the raster plots (predominantly red bottom panel), and channels with Ap onsets are shown in the upper part (predominantly blue top panel). Some channels had both Ap and Av onsets, in which case they are shown twice, once in each part of the raster plot.

In the bottom panels of Figure 6A, we show the group means of the normalized beta power time course of the channels that had either Ap or Av onsets. For each channel, power was normalized by the formula, [Power Magnitude - Baseline] / Baseline, where Baseline indicates the mean of the precue power. Of the 107 N-group channels, 64 channels had a choice discrimination onset (Ap and/or Av onsets) (left bottom panel in Figure 6A). For 193 P-group channels, 147 channels had discrimination onsets (right bottom panel in Figure 6A). For each time point of the population activity, a two-sided t-test was performed to examine whether the power magnitude exhibited significant difference between Ap (blue) and Av (red) trials. Colored highlights of x-axis at the bottom of the figure indicate the time when the population activity was significantly different ($p < 0.05$) between approach and avoidance trials with higher magnitude for Ap (blue) or for Av (red) choices.

Classification of Beta Responses Recorded during the *Stim-on*, *Follow-up* and *Recovery* Blocks—In Figure 7B, we show the analysis of the beta responses recorded in the *Stim-on*, *Follow-up* and *Recovery* blocks. We selected channels that were task-related in the *Stim-off* and/or *Follow-up* blocks and from which we could stably record the LFPs continuously from the *Stim-off* to *Recovery* blocks (Table S1). From the 84 channels in the negative effective sessions, we thus had 84 additional recordings in each of the *Stim-on*,

Follow-up and *Recovery* blocks (84 × 3 = 252 additional recordings in the three blocks). In order to classify these 252 beta responses recorded in the three blocks of the effective sessions, we combined the 252 beta responses with the original 667 *Stim-off* beta responses ('combined set'). We then performed MDS to derive the relative similarities among the combined set. The number of groups assigned to the combined set was again five. The results of the classification of 252 beta responses in other blocks are shown in Figure 7B. Importantly, we confirmed that, even though we added the 252 beta responses to produce the combined set, the results for the original 667 beta responses in the combined set were almost the same as when they were classified by themselves. The differences between PCVs for the combined set and the original set were negligible, indicating that the PCVs and the groups assigned to the combined set correspond to those assigned to the original set (Figure 7A). Similarly, for the 90 channels recorded in the non-effective sessions, we recorded 90 beta responses in the *Stim-on* and 90 beta responses in the *Follow-up* blocks (i.e., 180 beta responses in total), in addition to the original 90 beta responses in the *Stim-off* block. To derive the groups of the 180 beta responses in relation to the groups assigned to the 667 original *Stimoff* beta responses, we combined the 180 beta responses with the original 667 *Stim-off* beta responses to produce the combined set, and performed the classification. The classification also derived five groups, and the differences between the results obtained from the original set and the combined set were also negligible. These results indicate that the five groups assigned to the *Stim-on*, *Follow-up* and *Recovery* beta responses were the same as the five groups assigned for the *Stim-off* beta responses.

Power Spectra for N-f Channels—Figures S8A–S8D show the power spectra for N-f channels and Av-Ap tuning indices. For each channel, the cue-period power spectra were derived for Ap and Av choices as $G_{AP}(f)$ and $G_{AV}(f)$. These values were normalized as $N_{AP}(f)=G_{AP}(f)/M$ and $N_{AV}(f)=G_{AV}(f)/M$, where $M=\overline{G_{AP}}$ is the averaged value over f. Figure 8 shows the population means of $N_{AP}(f)$ and $N_{AV}(f)$ of N-f and the other channels. The Av-Ap tuning index for each channel was calculated by $T(f)=(G_{AV}(f)-G_{AP}(f))/M$. In each block, we tested whether the population mean of $T(f)$ was significantly different from that in the *Stim-off* block (two-sampled t-test). For each frequency point, we set the significance level to be $0.05/m$, where m is the number of independent frequency points, which we estimated as the width of the beta band divided by the smoothing bandwidth of the taper set (Bonferroni correction).

Definition of Differential Beta Responses during the Precue Period—Figure 8 illustrates the precue beta activity differentiating previous Ap-Av choices. To obtain these values, we first defined the peak frequency at which the beta power is maximally different from the pink noise baseline. If the beta power at the peak frequency showed significant difference in magnitude between previous Ap and previous Av choices ($p < 0.05$, two-tailed z-test), we defined the precue beta activity as representing previous choices. Beta activities recorded on 16 channels exhibited significant increases for the previous Av choices in one of three blocks, and those recorded on 7 channels showed significant increases for the previous Ap choices. We derived the power spectra for these channels similarly to those for N-f channels.

Supplementary Material

Refer to Web version on PubMed Central for supplementary material.

ACKNOWLEDGMENTS

We thank Drs. Eberhard Fetz, Robert Desimone and Diego Pizzagalli for critical reading of earlier drafts of this manuscript, Drs. Simon Hong, Hideki Shimazu and Helen Schwerdt for experimental interactions, Margo Cantor, Jonathan Gill and Caitlin Erickson for help with monkey training, Dr. Tomoko Yoshida and Emily Chung for help with histology, Henry Hall for help with many aspects of this work, and Dr. Yasuo Kubota for help with manuscript preparation. This research was supported by the National Institutes of Health (R01 NS025529), the CHDI Foundation (A-5552), the Office of Naval Research (N00014-07-1-0903), the Army Research Office (W911NF-16-1-0474), MEXT KAKENHI (18H04943, 18H05131), the Simons Center for the Social Brain, the Naito Foundation, the Uehara Memorial Foundation, P. Dana Bartlett, Robert Buxton, Amy Sommer, and Judy Goldberg.

REFERENCES

Ahmari SE, Spellman T, Douglass NL, Kheirbek MA, Simpson HB, Deisseroth K, Gordon JA, and Hen R (2013). Repeated cortico-striatal stimulation generates persistent OCD-like behavior. Science 340, 1234–1239. [PubMed: 23744948]

Amemori K, Amemori S, and Graybiel AM (2015a). Motivation and affective judgments differentially recruit neurons in the primate dorsolateral prefrontal and anterior cingulate cortex. J Neurosci 35, 1939–1953. [PubMed: 25653353]

Amemori K, Gibb LG, and Graybiel AM (2011). Shifting responsibly: the importance of striatal modularity to reinforcement learning in uncertain environments. Front Hum Neurosci 5, 47. [PubMed: 21660099]

Amemori K, and Graybiel AM (2012). Localized microstimulation of primate pregenual cingulate cortex induces negative decision-making. Nat Neurosci 15, 776–785. [PubMed: 22484571]

Amemori S, Amemori K, Cantor ML, and Graybiel AM (2015b). A non-invasive head-holding device for chronic neural recordings in awake behaving monkeys. J Neurosci Methods 240, 154–160. [PubMed: 25448381]

Aosaki T, Miura M, Suzuki T, Nishimura K, and Masuda M (2010). Acetylcholine-dopamine balance hypothesis in the striatum: an update. Geriatr Gerontol Int 10, S148–157. [PubMed: 20590830]

Aupperle RL, Melrose AJ, Francisco A, Paulus MP, and Stein MB (2015). Neural substrates of approach-avoidance conflict decision-making. Hum Brain Mapp 36, 449–462. [PubMed: 25224633]

Aupperle RL, Sullivan S, Melrose AJ, Paulus MP, and Stein MB (2011). A reverse translational approach to quantify approach-avoidance conflict in humans. Behav Brain Res 225, 455–463. [PubMed: 21843556]

Bakic J, Jepma M, De Raedt R, and Pourtois G (2014). Effects of positive mood on probabilistic learning: behavioral and electrophysiological correlates. Biol Psychol 103, 223–232. [PubMed: 25265572]

Boileau B (2011). A review of obsessive-compulsive disorder in children and adolescents. Dialogues Clin Neurosci 13, 401–411. [PubMed: 22275846]

Bokil H, Andrews P, Kulkarni JE, Mehta S, and Mitra PP (2010). Chronux: a platform for analyzing neural signals. J Neurosci Methods 192, 146–151. [PubMed: 20637804]

Brazhnik E, Shah F, and Tepper JM (2008). GABAergic afferents activate both GABAA and GABAB receptors in mouse substantia nigra dopaminergic neurons in vivo. J Neurosci 28, 10386–10398. [PubMed: 18842898]

Burguiere E, Monteiro P, Feng G, and Graybiel AM (2013). Optogenetic stimulation of lateral orbitofronto-striatal pathway suppresses compulsive behaviors. Science 340, 1243–1246. [PubMed: 23744950]

Canales JJ, and Graybiel AM (2000). A measure of striatal function predicts motor stereotypy. Nat Neurosci 3, 377–383. [PubMed: 10725928]

Cavanagh JF, Wiecki TV, Cohen MX, Figueroa CM, Samanta J, Sherman SJ, and Frank MJ (2011). Subthalamic nucleus stimulation reverses mediofrontal influence over decision threshold. Nat Neurosci 14, 1462–1467. [PubMed: 21946325]

Chen CH, Ridler K, Suckling J, Williams S, Fu CH, Merlo-Pich E, and Bullmore E (2007). Brain imaging correlates of depressive symptom severity and predictors of symptom improvement after antidepressant treatment. Biol Psychiatry 62, 407–414. [PubMed: 17217921]

Clarke HF, Dalley JW, Crofts HS, Robbins TW, and Roberts AC (2004). Cognitive inflexibility after prefrontal serotonin depletion. Science 304, 878–880. [PubMed: 15131308]

Clarke HF, Robbins TW, and Roberts AC (2008). Lesions of the medial striatum in monkeys produce perseverative impairments during reversal learning similar to those produced by lesions of the orbitofrontal cortex. J Neurosci 28, 10972–10982. [PubMed: 18945905]

Crittenden JR, Tillberg PW, Riad MH, Shima Y, Gerfen CR, Curry J, Housman DE, Nelson SB, Boyden ES, and Graybiel AM (2016). Striosome-dendron bouquets highlight a unique striatonigral circuit targeting dopamine-containing neurons. Proc Natl Acad Sci U S A 113, 11318–11323. [PubMed: 27647894]

Ding L, and Gold JI (2012). Separate, causal roles of the caudate in saccadic choice and execution in a perceptual decision task. Neuron 75, 865–874. [PubMed: 22958826]

Eblen F, and Graybiel AM (1995). Highly restricted origin of prefrontal cortical inputs to striosomes in the macaque monkey. J Neurosci 15, 5999–6013. [PubMed: 7666184]

Eldar E, and Niv Y (2015). Interaction between emotional state and learning underlies mood instability. Nat Commun 6, 6149. [PubMed: 25608088]

Eldar E, Rutledge RB, Dolan RJ, and Niv Y (2016). Mood as representation of momentum. Trends Cogn Sci 20, 15–24. [PubMed: 26545853]

Engel AK, and Fries P (2010). Beta-band oscillations-signalling the status quo? Curr Opin Neurobiol 20, 156–165. [PubMed: 20359884]

Feingold J, Desrochers TM, Fujii N, Harlan R, Tierney PL, Shimazu H, Amemori K, and Graybiel AM (2012). A system for recording neural activity chronically and simultaneously from multiple cortical and subcortical regions in nonhuman primates. J Neurophysiol 107, 1979–1995. [PubMed: 22170970]

Frank MJ, Woroch BS, and Curran T (2005). Error-related negativity predicts reinforcement learning and conflict biases. Neuron 47, 495–501. [PubMed: 16102533]

Friedman A, Homma D, Bloem B, Gibb LG, Amemori K, Hu D, Delcasso S, Truong TF, Yang J, Hood AS, et al. (2017). Chronic stress alters striosome-circuit dynamics, leading to aberrant decision-making. Cell 171, 1191–1205. [PubMed: 29149606]

Friedman A, Homma D, Gibb LG, Amemori K, Rubin SJ, Hood AS, Riad MH, and Graybiel AM (2015). A corticostriatal path targeting striosomes controls decision-making under conflict. Cell 161, 1320–1333. [PubMed: 26027737]

Fujiyama F, Sohn J, Nakano T, Furuta T, Nakamura KC, Matsuda W, and Kaneko T (2011). Exclusive and common targets of neostriatofugal projections of rat striosome neurons: a single neuron-tracing study using a viral vector. Eur J Neurosci 33, 668–677. [PubMed: 21314848]

Goldberg JA, Rokni U, Boraud T, Vaadia E, and Bergman H (2004). Spike synchronization in the cortex/basal-ganglia networks of Parkinsonian primates reflects global dynamics of the local field potentials. J Neurosci 24, 6003–6010. [PubMed: 15229247]

Graybiel AM (2008). Habits, rituals, and the evaluative brain. Annu Rev Neurosci 31, 359–387. [PubMed: 18558860]

Hikosaka O (2010). The habenula: from stress evasion to value-based decision-making. Nat Rev Neurosci 11, 503–513. [PubMed: 20559337]

Jenkinson N, and Brown P (2011). New insights into the relationship between dopamine, beta oscillations and motor function. Trends Neurosci 34, 611–618. [PubMed: 22018805]

Kim HF, and Hikosaka O (2013). Distinct basal ganglia circuits controlling behaviors guided by flexible and stable values. Neuron 79, 1001–1010. [PubMed: 23954031]

Korn CW, Vunder J, Miró J, Fuentemilla L, Hurlemann R, and Bach DR (2017). Amygdala lesions reduce anxiety-like behavior in a human benzodiazepine-densitive approach-avoidance conflict test. Biol Psychiatry 82, 522–531. [PubMed: 28364943]

Leventhal DK, Gage GJ, Schmidt R, Pettibone JR, Case AC, and Berke JD (2012). Basal ganglia beta oscillations accompany cue utilization. Neuron 73, 523–536. [PubMed: 22325204]

Lipsman N, Kaping D, Westendorff S, Sankar T, Lozano AM, and Womelsdorf T (2014). Beta coherence within human ventromedial prefrontal cortex precedes affective value choices. Neuroimage 85, 769–778. [PubMed: 23732884]

Luppino G, Matelli M, Camarda RM, Gallese V, and Rizzolatti G (1991). Multiple representations of body movements in mesial area 6 and the adjacent cingulate cortex: an intracortical microstimulation study in the macaque monkey. J Comp Neurol 311, 463–482. [PubMed: 1757598]

McCarthy MM, Moore-Kochlacs C, Gu X, Boyden ES, Han X, and Kopell N (2011). Striatal origin of the pathologic beta oscillations in Parkinson's disease. Proc Natl Acad Sci U S A 108, 11620–11625. [PubMed: 21697509]

Merkl A, Neumann W-J, Huebl J, Aust S, Horn A, Krauss JK, Dziobek I, Kuhn J, Schneider G-H, Bajbouj M, and Kühn AA (2015). Modulation of beta-band activity in the subgenual anterior cingulate cortex during emotional empathy in treatment-resistant depression. Cereb Cortex 26, 2626–2638. [PubMed: 25994959]

Millan MJ (2003). The neurobiology and control of anxious states. Prog Neurobiol 70, 83–244. [PubMed: 12927745]

Nakamura K, and Hikosaka O (2006). Facilitation of saccadic eye movements by postsaccadic electrical stimulation in the primate caudate. J Neurosci 26, 12885–12895. [PubMed: 17167079]

Pizzagalli DA (2011). Frontocingulate dysfunction in depression: toward biomarkers of treatment response. Neuropsychopharmacology 36, 183–206. [PubMed: 20861828]

Price JL, and Drevets WC (2012). Neural circuits underlying the pathophysiology of mood disorders. Trends Cogn Sci 16, 61–71. [PubMed: 22197477]

Rajakumar N, Elisevich K, and Flumerfelt BA (1993). Compartmental origin of the striato-entopeduncular projection in the rat. J Comp Neurol 331, 286–296. [PubMed: 8509503]

Ruscio AM, Stein DJ, Chiu WT, and Kessler RC (2010). The epidemiology of obsessive-compulsive disorder in the National Comorbidity Survey Replication. Mol Psychiatry 15, 53–63. [PubMed: 18725912]

Saka E, Goodrich C, Harlan P, Madras BK, and Graybiel AM (2004). Repetitive behaviors in monkeys are linked to specific striatal activation patterns. J Neurosci 24, 7557–7565. [PubMed: 15329403]

Steel Z, Marnane C, Iranpour C, Chey T, Jackson JW, Patel V, and Silove D (2014). The global prevalence of common mental disorders: a systematic review and meta-analysis 1980–2013. Int J Epidemiol 43, 476–493. [PubMed: 24648481]

Train K (2003). Discrete choice methods with simulation (New York: Cambridge University Press).

Watanabe M, and Munoz DP (2010). Saccade suppression by electrical microstimulation in monkey caudate nucleus. J Neurosci 30, 2700–2709. [PubMed: 20164354]

Williams ZM, and Eskandar EN (2006). Selective enhancement of associative learning by microstimulation of the anterior caudate. Nat Neurosci 9, 562–568. [PubMed: 16501567]

Worbe Y, Epinat J, Féger J, and Tremblay L (2011). Discontinuous long-train stimulation in the anterior striatum in monkeys induces abnormal behavioral states. Cereb Cortex 21, 2733–2741. [PubMed: 21508304]

Highlights

- Caudate N. stimulation induces persistent state-change affecting value evaluation
- CN stimulation produces repetitive choices, whereas pACC stimulation does not
- CN beta oscillations parallel negative states influencing repetitive decisions
- Abnormal CN beta oscillations is correlated with persistency in OCD-like states

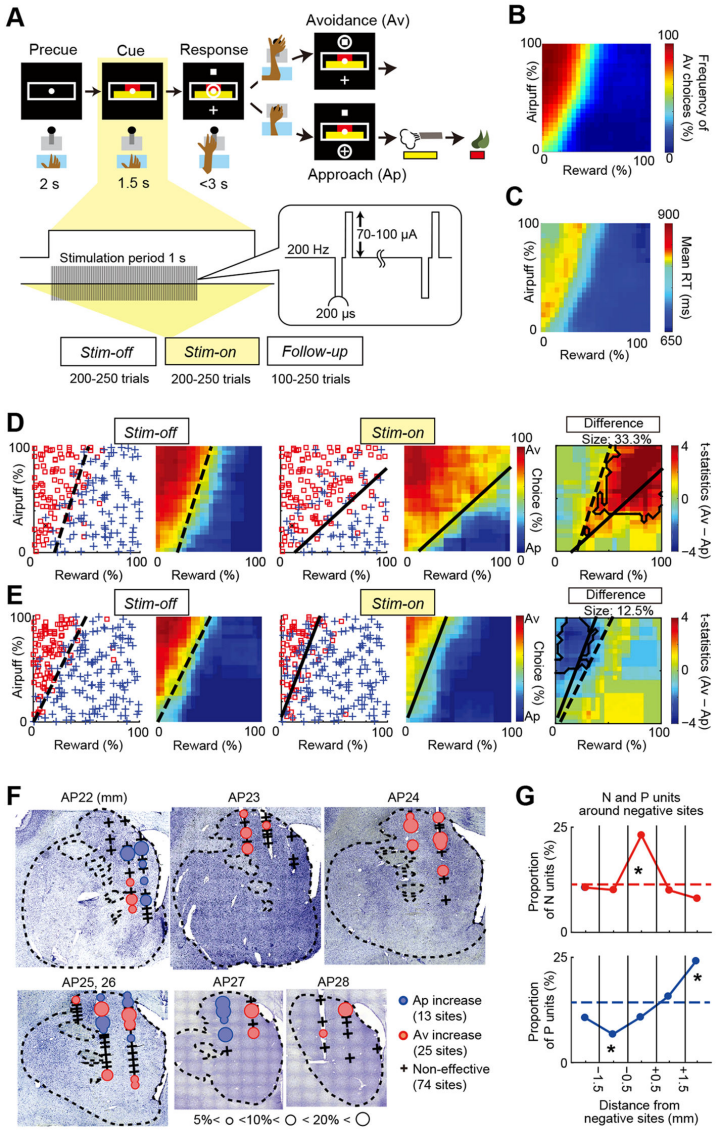

Figure 1. The Ap-Av Task and the CN Microstimulation Effects

(A) Task procedure and experimental blocks. During the cue period, the red and yellow horizontal bars, respectively signaling the offered amounts of reward and punishment, appeared on the monitor. The monkeys made a decision between acceptance and rejection of the combined offer, and reported this by choosing either of two targets (cross for acceptance; square for rejection) that appeared during the response period. The locations of the targets were alternated randomly.

(B) Mean Ap-Av choices.

(C) Mean reaction times.(D and E) Examples of negative

(D) and positive (E) stimulation effects. Ap (blue cross) and Av (red square) choices in the *Stim-off* (left panels) and *Stim-on* (middle panels) blocks in the same session and difference between these blocks (right panels). Decision matrices are plotted in left panels for the two blocks. Black contours in the right panels represent significant effect zones ($p < 0.05$,

Fisher's exact test). Dashed and solid lines in these panels respectively denote the decision boundaries in the *Stim-off* and *Stim-on* blocks.

(F) Distribution of the effective sites. Stimulation results mapped onto Nissl-stained coronal sections. Blue and red circles indicate sites at which microstimulation respectively induced an increase in Ap and Av. Black crosses indicate non-effective sites. The size of the circles indicates the size of the effects. Data from monkey S were projected onto those from monkey P.

(G) Proportions of N units (top) and P units (bottom) (number of N and P units / total number of recorded units), shown for 1-mm bins around the negative effective sites. Asterisk indicates the bin in which the proportion of N units or P units was significantly different from that of units aggregated over all tracks. *$p < 0.05$ (Fisher's exact test).

See also Figure S1.

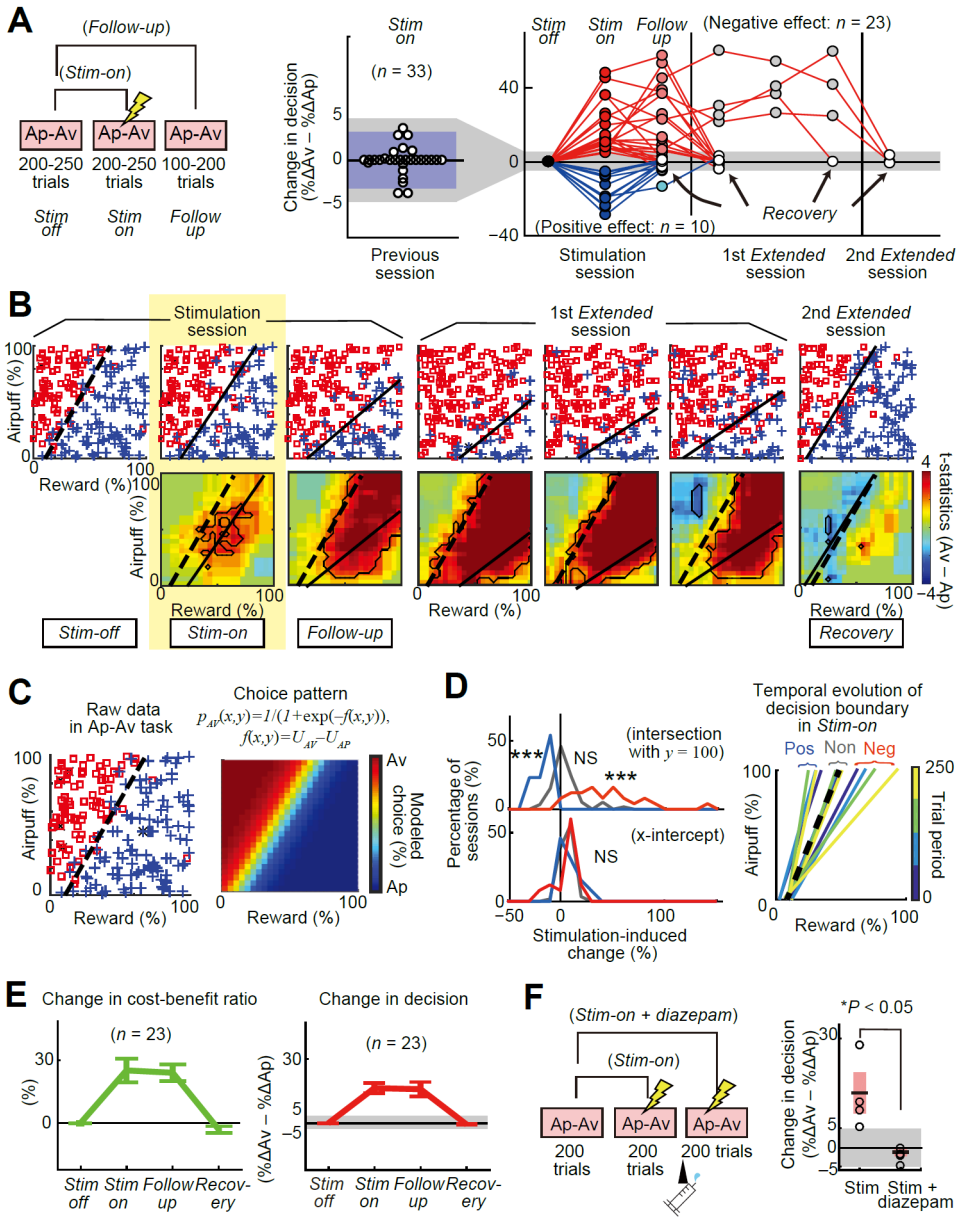

Figure 2. CN Microstimulation Induced Persistent Change in State Affecting Value Evaluation

(A) Changes in decision (%ΔAv - %ΔAp) across post-stimulation sessions. Stimulation-induced changes in decision were measured by comparing the decisions in the *Stim-off* and *Stim-on* blocks, and long-lasting effect was measured by comparing those in the *Stim-off* and *Follow-up* blocks (left). In the preceding sessions (middle), stimulation-induced changes in decision (white circles) were not significant. Purple region denotes the 95% confidence interval, and the upper limit was 3.3%. Gray shading extending from middle to right panels indicates the 5% significance threshold. After this control period, microstimulation induced increases in Av (red) or Ap (blue) decisions, relative to the *Stim-off* block (black), and some of these effects continued into *Extended sessions* (right). White circles: *Recovery* blocks. (B) Example of consecutive daily sessions. Stimulation induced increases in Av choices during the stimulation session (left panels) and the first *Extended session* (middle panels),

but not during the second *Extended session* (right panels). Top panels show choices plotted in decision matrix; bottom panels show changes in decision between *Stim-off* and designated blocks. Dashed and solid lines denote the decision boundaries in, respectively, *Stim-off* and other blocks. Each panel is illustrated as in Figure 1D.

(C) Econometric modeling. With the choice behavior in a single block (left), we performed logistic regression to construct a choice model (right).

(D) Stimulation effects on decision boundaries. Distribution of points of intersections of the decision boundary in the *Stim-on* blocks (left), shown as percentage of sessions of positive (blue), negative (red) and non-effective (gray) sites. Stimulation did not change the distribution of x-intercepts (bottom left), but induced significant changes in intersection with $y = 100$ for effective sessions (top left). Change in slope of the decision boundary in the negative (Neg), positive (Pos) and non-effective (Non) sessions, derived for 4 trial periods in the *Stim-on* blocks indicated by color scale at right (right). Black dashed line indicates the decision boundary in the *Stim-off* block. ***$p < 0.001$, NS: $p > 0.05$ (t-test).

(E) Summary of the negative stimulation effect. Mean changes in CBR (left) and decision (right) are plotted with changes in each block of consecutive sessions. Error bars indicate SEM. (F) Diazepam administration blocked stimulation-induced increase in Av choices. Left: Cartoon of protocol. Right: Diazepam significantly suppressed the negative effects (two-tailed t-test). Each data point (circle) was overlaid with 95% confidence interval (pink) and the mean (black).

See also Figures S2 and S3.

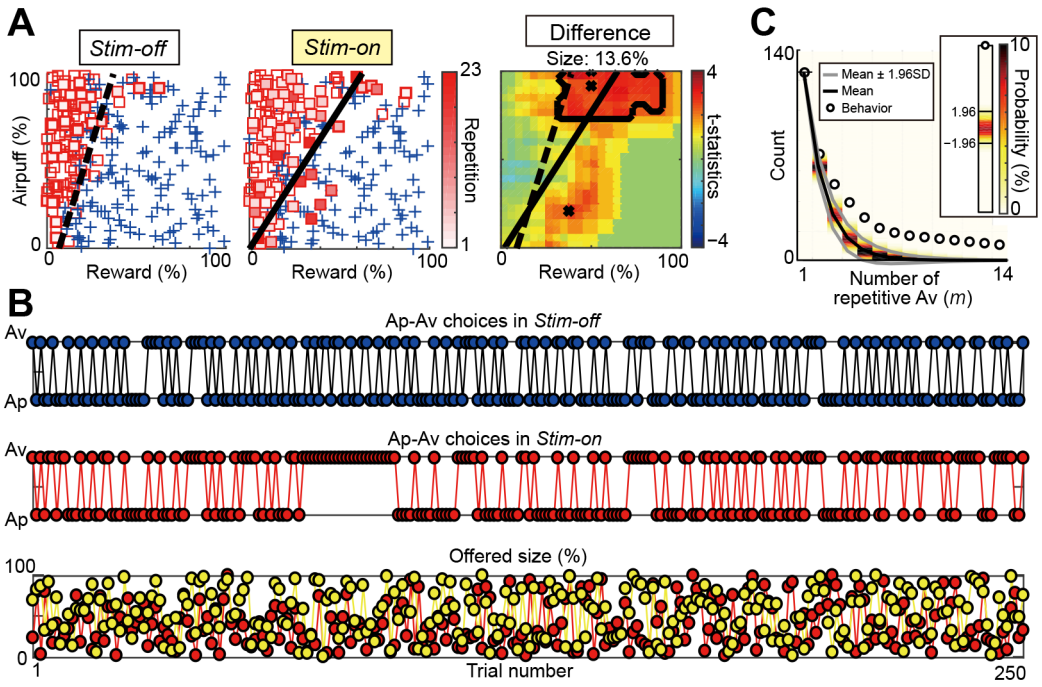

Figure 3. CN Microstimulation Increased Repetitive Av Choices

(A) Ap (blue crosses) and Av (red squares) decisions in the *Stim-off* (left) and *Stim-on* (middle) blocks in the same session, plotted in the decision matrix. The gradation of red squares corresponds to the number of consecutive Av choices, as indicated by scale at right. Dashed and solid lines respectively denote the decision boundaries in the *Stim-off* and *Stim-on* blocks. Right panel shows the difference between *Stim-off* and *Stim-on* blocks, illustrated as in Figure 1D.

(B) Decision sequences in the *Stim-off* (top) and *Stim-on* (middle) blocks. The bottom panel shows the sequence of the offered reward (red circles) and airpuff (yellow circles) sizes. The same sequence was used in the *Stim-off* and *Stim-on* blocks.

(C) Comparison between the observed number of repetition in the *Stim-on* block and the expected number of repetition derived from the RR procedure. Circles represent the counts of *m* repetitions of Av choice observed in the choice sequence. Black and gray lines show, respectively, the mean and the 95% confidence limit of the distribution produced by the RR procedure. Mean z-statistic representing deviation from the model is shown at right.

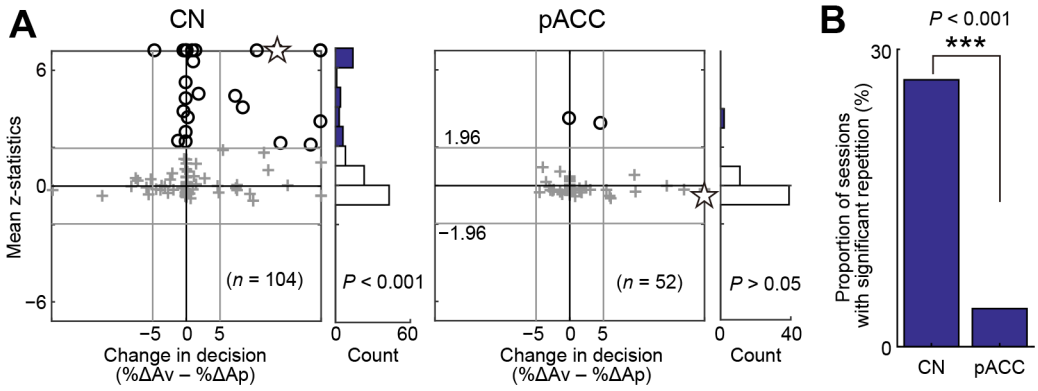

Figure 4. CN Microstimulation Induced Unusually Repetitive Choices, whereas pACC Microstimulation Did Not

(A) Mean deviation in repetitive Av choices, measured in z-statistic, representing the difference between the observed behavior and the prediction of the RR procedure during sessions with CN (left) or pACC (right) stimulation. X-axis indicates the size of changes in decision, calculated by the difference in positive and negative effects (%ΔAv − %ΔAp). Circles indicate the sessions in which the stimulation induced significant deviation from the RR prediction ($p < 0.05$, z-test), and gray crosses are non-significant sessions. Stars indicate the sessions shown in Figures 3 and S3. Data points beyond the range of the y-axis are shown at the ceiling. Bars at right show the distribution of the mean deviations.

(B) Proportion of sessions that had significant deviation ($p < 0.05$, z-test) from the prediction of the RR procedure. Proportion in the CN stimulation experiments was significantly larger than that in the pACC experiments (Fisher's exact test).

See also Figures S4–S6.

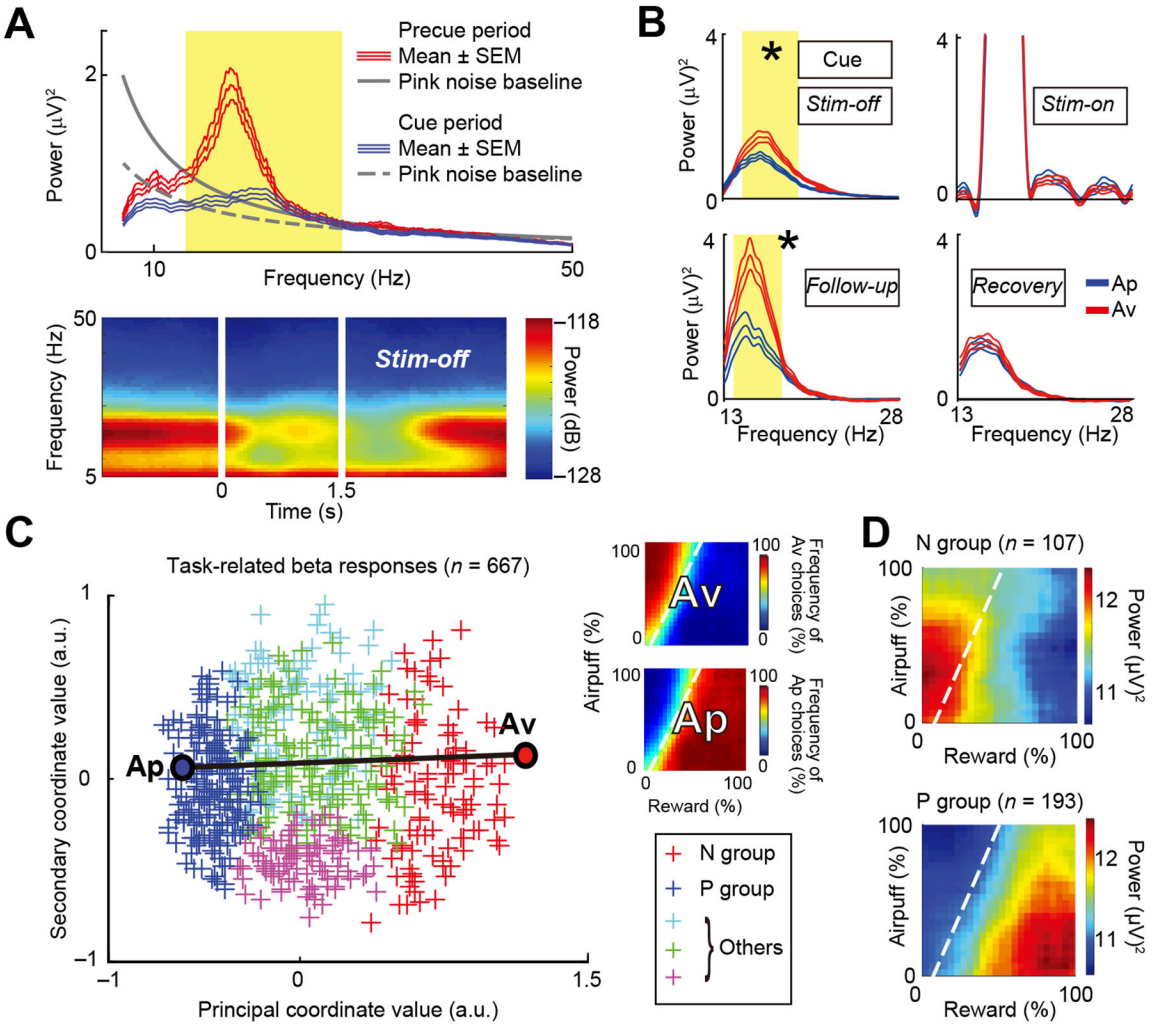

Figure 5. Beta Oscillations Represent Decision-Related Variables

(A) Example of power spectrum (top) and spectrogram (bottom) of task-related LFP activity. Red and blue lines in the top panel indicate the mean spectra (± SEM) for, respectively, the precue and cue periods. Yellow shading indicates the beta range (13–28 Hz). The gray line (solid: precue, dashed: cue) indicates the fitted pink noise baselines.

(B) Example of baseline-subtracted power spectra (± SEM) of the cue-period LFP activity that exhibited choice selectivity modulation during a negative effective session. Red and blue lines indicate the mean spectra (± SEM) for upcoming Av (red) and Ap (blue) choices, respectively. For each block, z-tests were performed between spectra for Ap and Av. Yellow shading indicates the frequency range with significant differences between Ap and Av in the power spectra. *$p < 0.05$ (z-test, Bonferroni corrected).

(C) Beta response matrices projected onto the first two dimensions of the MDS (MDS map). Each cross indicates individual channel. Color indicates the group to which the channel belongs (N group: red; P group: blue; and other groups: green, cyan and magenta). To examine the similarity of each beta response to the behavioral choice pattern, MDS was performed with the Ap and Av behavioral responses shown on the right. The position of behavioral Ap choice (top right matrix) was at the leftmost position, and that of Av choice

(bottom right matrix) at the rightmost position in the MDS map, indicating that the principal coordinate value (i.e., PCV) represents Av-Ap tuning of each beta response.
(D) Mean beta responses of N (top) and P (bottom) groups plotted in decision matrices. Dashed lines: decision boundaries.
See also Figure S7.

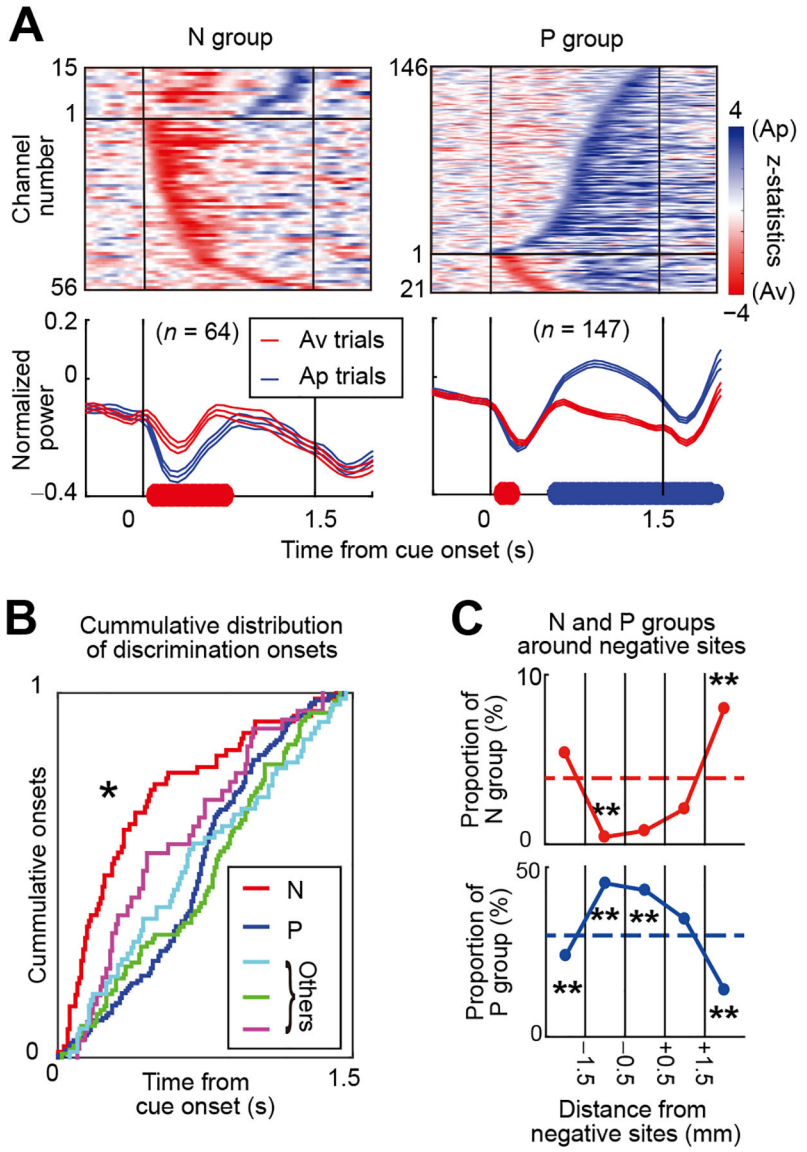

Figure 6. Properties of the Beta Responses That Belong to N and P Groups

(A) Time-course of the z-values (top, Wilcoxon rank-sum test) and power (bottom, mean ± SEM normalized by precue activity) of beta responses that discriminated upcoming Av (red) and Ap (blue) choices and that were categorized as N (left) or P (right) groups. Colored highlights on x-axis show significantly larger magnitudes for Av (red) or Ap (blue) choice ($p < 0.05$, two-tailed t-test).

(B) Cumulative onset times at which beta responses discriminated upcoming choices, showing significantly earlier onset in N group (red) than in the others. *$p < 0.05$ (Kolmogorov-Smirnov test).

(C) Proportions of N-group (top) and P-group (bottom) beta responses (number of beta in each group / total number of recorded beta), shown for 1-mm bins around the negative effective sites. Asterisk indicates the bin in which the proportion of N-group or P-group beta

response was significantly different from that of beta responses aggregated over all tracks.
**p < 0.01 (Fisher's exact test).
See also Figure S7.

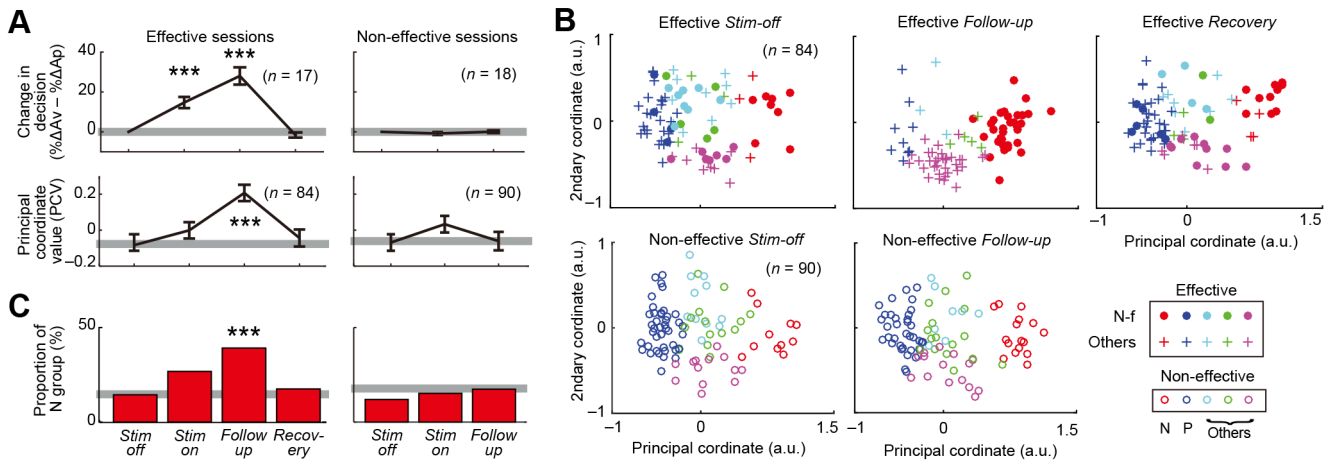

Figure 7. Changes of Beta Representation Coincide with Behavioral Effects of CN Microstimulation

(A) Mean (± SEM) change in decision frequencies (top) and PCVs of cue-period beta responses (bottom) for effective (left) and non-effective (right) sessions. Mean PCV in the *Follow-up* block of effective sessions was significantly larger than that in recording-only sessions (gray line), but not in non-effective sessions. ***p < 0.001 (two-tailed t-test).

(B) Classifications of the 84 beta responses in effective sessions (top) and those of 90 beta responses in non-effective sessions (bottom). Filled circles: beta responses of N-f channels in effective sessions. Crosses: the others in effective sessions. Open circles: beta responses in non-effective sessions. Colors show beta responses categorized as N (red), P (blue), and other (green, cyan and magenta) groups in the block indicated above each plot.

(C) Proportion of N group for each block of effective (left) and non-effective (right) sessions, with significant increase in the *Follow-up* block relative to the proportion of N group in recording-only sessions (gray line). ***p < 0.001 (Fisher's exact test).

See also Figure S8.

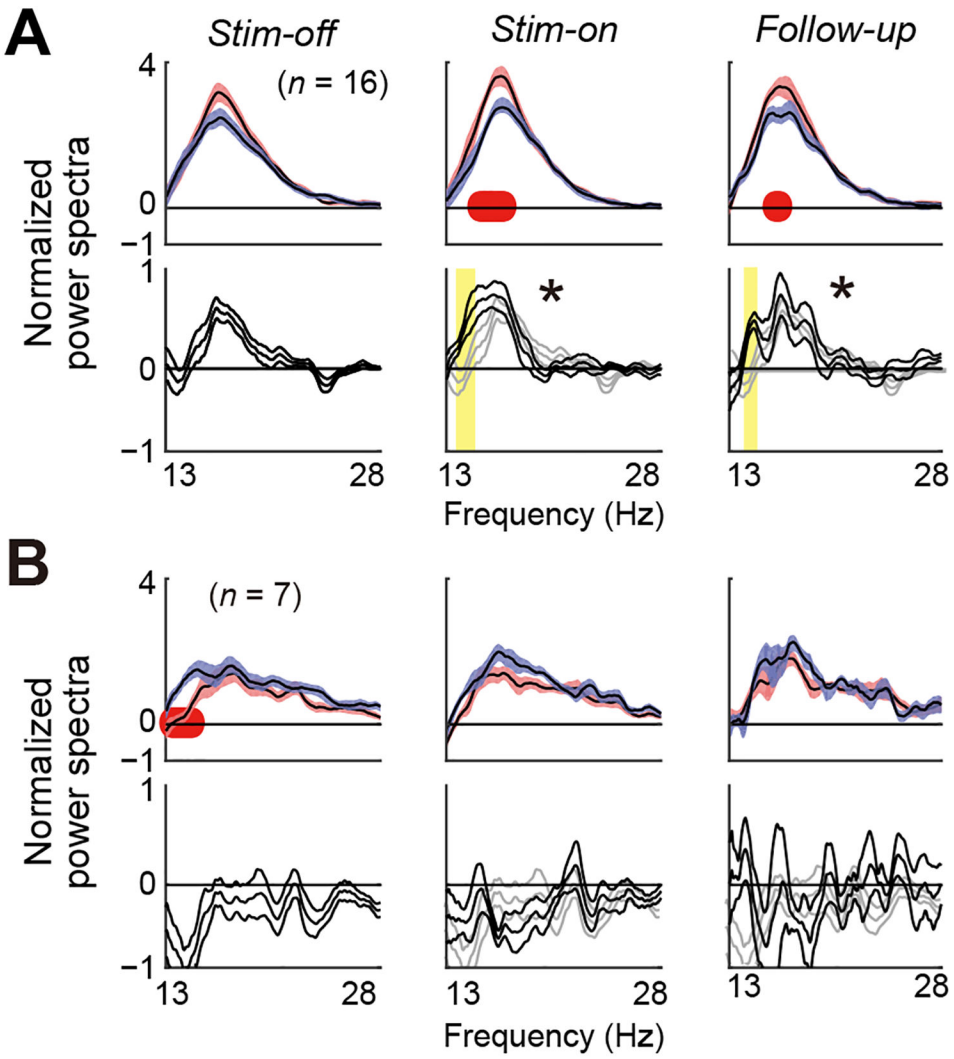

Figure 8. Modulation of Power Spectra in Abnormally Repetitive Sessions

(A) Precue power spectra of 16 channels that showed significant elevation for previous Av choice. Top: Mean (± SEM) power spectra for previous Ap (blue) and for previous Av (pink) choices. Bottom: Mean (± SEM) tuning indices derived by subtracting spectrum for previous Av from that for previous Ap spectra (black). Yellow shading indicates significant increase in the tuning index from that in the *Stim-off* block (gray). *$p < 0.05$ (t-test, Bonferroni corrected).

(B) Precue power spectra of 7 channels that showed significant elevation for previous Ap choice.